

Nearly Optimal Bayesian Inference for Structural Missingness

Chen Liang¹ Donghua Yang¹ Yutong Zhao¹ Tianle Zhang¹ Shenghang Zhou¹ Zhiyu Liang¹
 Hengtong Zhang¹ Hongzhi Wang¹ Ziqi Li¹ Xiyang Zhang¹ Zheng Liang¹ Yifei Li¹

Abstract

Structural missingness breaks 'just impute and train': values can be undefined by causal or logical constraints, and the mask may depend on observed variables, unobserved variables (MNAR), and other missingness indicators. It simultaneously brings (i) a *catch-22 situation with causal loop*, prediction needs the missing features, yet inferring them depends on the missingness mechanism, (ii) under MNAR, *the unseen are different*, the missing part can come from a shifted distribution, and (iii) plug-in imputation, a single fill-in can lock in uncertainty and yield overconfident, biased decisions. In the Bayesian view, prediction via the posterior predictive distribution integrates over the full model posterior uncertainty, rather than relying on a single point estimate. This framework decouples (i) learning an *in-model* missing-value posterior from (ii) label prediction by optimizing the predictive posterior distribution, enabling posterior integration. This decoupling yields an in-model *almost-free-lunch*: once the posterior is learned, prediction is plug-and-play while preserving uncertainty propagation. It achieves SOTA on 43 classification with missing data and 15 imputation benchmarks, with finite-sample near Bayes-optimality guarantees under our SCM prior.

1. Introduction

Structural Missingness. In many real-world applications, data is often incomplete due to various reasons such as sensor failures, terms of data collection, or privacy concerns. Rubin's theory of missing data (Rubin, 1976) proposed a framework for handling missing data, where the missing data is assumed to be (1) missing completely at random (MCAR), where the missingness is independent of the ob-

¹Harbin Institute of Technology, Harbin, China. Correspondence to: Hongzhi Wang <wangzh@hit.edu.cn>, Donghua Yang <yang.dh@hit.edu.cn>.

served and unobserved variables, (2) missing at random (MAR), where the missingness is dependent on the observed variables, or (3) missing not at random (MNAR), where the missingness is dependent on the unobserved variables.

Since MCAR/MAR/MNAR classify missingness by whether M depends on observed/unobserved entries of X , we focus on *structural missingness*: some values are *logically undefined* and masks can exhibit within-mask dependencies (edges $M \rightarrow M$) (Mitra et al., 2023). In our scope, we model this via a second-order SCM with randomized missingness mechanisms but a fixed Markov structure, in Sec. 4.

Though previous missingness types provides a framework for understanding missing data, reaching a joint solution for fitting the properties of the above missingness types without bias has many challenges as follows:

Challenge 1: Alleviating MNAR bias is still an open problem. Bias may be caused *only under MNAR* by adopting the assumption that observed and unobserved variables have identical distributions, and this issue does not arise under MCAR/MAR (Muzellec et al., 2020). Under MNAR, the missingness mechanism depends on unobserved values, so the conditional distribution of missing features given observations can be shifted relative to the observed part and is not identifiable without structural assumptions. We make these assumptions explicit via our second-order SCM prior (Sec. 4, in Remark 6.6) (Muzellec et al., 2020; Vo et al., 2024; Zhang et al., 2025). We summarize this as: $P(x | M = 1)$, values that end up missing, can differ from $P(x | M = 0)$, values that are observed. Consequently, standard practice, i.e., training and predicting as if missingness were MAR/ignorable, or filling in a single point estimate (often implicitly treating missing values as drawn from $P(x | M = 0)$), can induce systematic prediction bias, which is named **MNAR bias**.

Challenge 2: Obstacles in Explicit Modeling for Prior Distribution. Even with powerful function approximators, learning from partial observations still requires introducing prior knowledge. This challenge has two parts:

(1) *Explicit prior modeling is hard*: the prior must be both flexible and tractable. Structural causal models can en-

code Markovian properties (Pearl, 2009; Spirtes & Glymour, 1991; Spirtes et al., 2000), but they often rely on independence testing assumptions and scale poorly, so expert knowledge is typically required in highly structured settings (Pearl, 2009).

(2) *Uncertainty over prior knowledge is harder*: the bottleneck is *specifying* the right prior, which becomes a near ‘chicken-and-egg’ problem when manually encoding what is known vs. unknown (Vo et al., 2024).

We show that, despite this need for manual prior design in highly structured settings (Pearl, 2009), a PFN-style ‘causal ladder’ view (Hollmann et al., 2022) motivates a level-1.5 *in-model* ‘almost-free-lunch’: not unconstrained causal discovery, but amortized identification of missingness/causal dependencies for prediction under a second-order SCM prior (Balazadeh et al., 2025; Robertson et al., 2025).

Challenge 3: Dealing with Uncertainty for Structural Missingness. Traditional approaches often rely on *deterministic* imputation to fill in missing values. However, *even if* one had a reasonable prior/mechanism in mind, plug-in imputation does not fully leverage the prior/posterior support. Instead of integrating over significant possible missing values in the downstream task, it commits to a single fill-in and loses uncertainty propagation.

In conclusion, under structural missingness it is difficult to specify or integrate prior knowledge that faithfully captures the dependencies between missing and observed/unobserved variables across arbitrary tasks, which is named **plug-in imputation bias**, leading to suboptimal performance. The question leaves:

How can we address the three challenges in practice in a single, two-birds-with-one-seed unified efficient framework?

Our Approach. *Bayesian inference is both necessary and sufficient* for the above challenges: to be correct under MNAR and avoid plug-in imputation bias, a predictor must reason about the *uncertainty* of unobserved variables, rather than committing to a single imputed input, after which optimal prediction follows from standard Bayesian principles as demonstrated in Sec. 3. We make this view practical by constructing a prior distribution over the missingness model and causal mechanisms in Sec. 4, and learning an implicit posterior-predictive map from incomplete inputs, with an optional missing-value posterior for sampling, in Sec. 5.

We formalize the task and derive the Bayesian predictive formulation in Sec. 2 and Sec. 3, and discuss near Bayes-optimality via a finite-sample excess-risk bound in Sec. 6. Finally, we validate the method in two real-world experimental suites for classification and imputation in Sec. 7.

For conceptual background, we provide a comprehensive related-work discussion in Sec. A.

Contributions.

1. We formulate classification with structural missingness as posterior predictive inference conditioned on the observed subspace and the mask, unifying MCAR/MAR/MNAR (**addresses Challenge 2**).
2. We propose posterior integration for prediction via a PFN (nearly optimal under the prior, **addresses Challenge 3**), with an optional learned missing-value posterior for sampling/analysis, propagating uncertainty and avoiding plug-in imputation bias and MNAR bias (**addresses Challenge 1**).
3. We give a finite-sample risk bound that decomposes posterior-approximation and predictor errors, explaining plug-in bias and MNAR bias and implying lower sample complexity to reach a target error than plug-in/imputation baselines.

Code and scripts will be released upon acceptance.

2. Problem Definition

We consider a training dataset $D = \{(x_i, y_i)\}_{i=1}^N$, where each $x_i \in \mathbb{R}^d$ represents a feature vector and $y_i \in \{1, \dots, C\}$ is the corresponding class label. The feature vectors are subject to structural missingness, denoted by a binary mask $M_i \in \{0, 1\}^d$, where $M_{ij} = 1$ indicates that the j -th feature of the i -th sample is missing, and $M_{ij} = 0$ indicates it is observed. Our goal is (1) to make tractable inference for the missing variables X_m given the observed variables X_m^c and the mask M and (2) to learn a predictor $p(y | x, D)$ for a new test feature vector x governed by a specific mask m , utilizing the information from the training dataset D and its associated collection of masks $\{M_i\}_{i=1}^N$.

Example (classification with missing features). Consider binary disease prediction from an incomplete patient record. Each patient has a latent complete feature vector $x \in \mathbb{R}^d$ (e.g., labs and survey answers) and label $y \in \{0, 1, \dots, k\}$, but at test time we only observe (x_m^c, m) . The task is to output a calibrated classifier for the label conditioned on what is actually observed under the given structural missingness pattern.

In the next section (Sec. 3), we give the Bayesian formulation of this problem definition by expressing prediction as posterior predictive inference conditioned on the observed subspace and the mask.

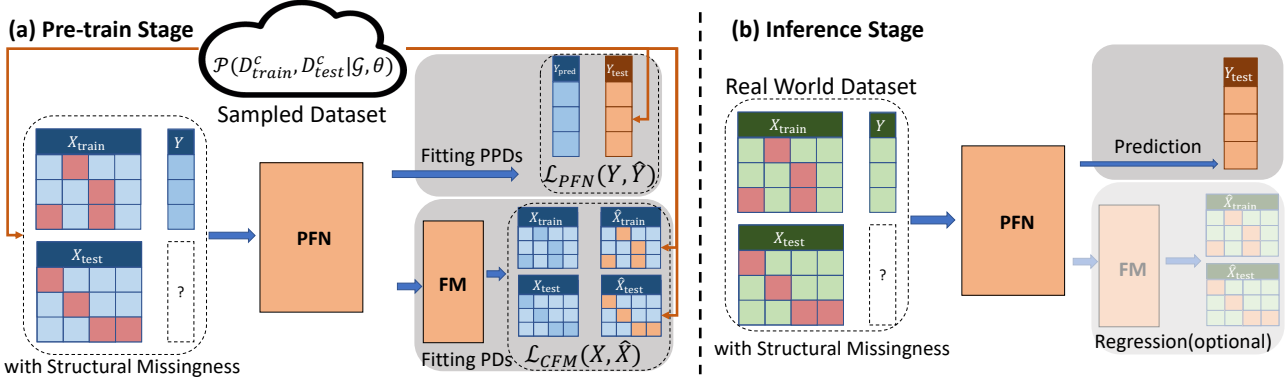


Figure 1. Overview of the training and inference framework. In pre-training, inputs ($X_{\text{train}}, X_{\text{test}}$) are incomplete (with masks M), sampled from the causal model in Sec. 4.1 and Fig. 2. The PFN is trained end-to-end to output the *in-model* posterior predictive distribution (PPD) directly from incomplete inputs (i.e., it implicitly marginalizes over missing values under the SCM prior), and predicts y_{test} for the corresponding incomplete X_{test} . In addition, a Flow Matching head can be trained to model a PD over missing values for explicit sampling/imputation and uncertainty analysis, but label prediction uses the PFN output and does not require Monte Carlo over completions.

3. Bayesian Inference with Structural Missingness

We define the missing variable X_m and the observed variable X_m^c as stochastic projections of the complete data dependent on the realization of M . Let $\text{Proj} : (M, X) \mapsto X_m$ denote the projection operator that maps a vector to the subspace indexed by set S . We formally define:

$$\begin{aligned} X_m &:= \text{Proj}(M, \mathbf{X}) \\ X_m^c &:= (\text{Proj}(M_c, \mathbf{X}), M) \end{aligned} \quad (1)$$

Note that X_m^c explicitly includes the mask M , ensuring that the "observation" includes information about which variables are observed. X_m and X_m^c are still well-defined random variables to perform Bayesian inference. The formal proof that X_m and X_m^c constitute valid random variables on the appropriate disjoint union spaces is provided in Appendix C.1.

Consider a dataset of n independent and identically distributed samples, partitioned into observed and missing components: $D_m^c = \{(X_{m,i}^c, y_i)\}_{i=1}^n$ and $D_m = \{X_{m,i}\}_{i=1}^n$. We assume a prior distribution over the missing parameters (or latent variables). The inference goal is to compute the posterior predictive distribution of the target y given the observed history D_m^c and the current observation X_m^c .

Predictive Posterior Distribution (PPD). Thus the regular conditional probability formula is still valid for the calculation of the predictive distribution. The predictive distribution is obtained by marginalizing over the *posterior distribution* of the missing data:

$$p(y|X_m^c, D_m^c) = \int_{X_m, D_m} \underbrace{p(y|X_m^c, X_m, D_m^c, D_m)}_{\text{General Situation}} dP(X_m, D_m|X_m^c, D_m^c) \underbrace{P(X_m, D_m|X_m^c, D_m^c)}_{\text{PD of Missing Data}} \quad (2)$$

This formulation allows us to decompose the complex problem of structural missingness into two distinct, manageable components as shown in Eq. (2).

Predictive Distribution without missingness. The first term, $p(y|X_m^c, X_m, D_m^c, D_m)$, represents the *general situation*: the standard predictive task where complete data is available. Since X_m^c and X_m together reconstruct the full feature vector \mathbf{X} (and similarly for the dataset D), this term reduces to the likelihood of the label given complete features, which is the domain of standard supervised learning models.

Posterior Distribution (PD) of the missing data. The second term, $P(X_m, D_m|X_m^c, D_m^c)$, represents the *posterior distribution (PD) of the missing data*. This term encapsulates the uncertainty regarding the unobserved features given the observed evidence and the specific missingness pattern. Evaluating the predictive distribution therefore hinges on our ability to model and making more accurate inference on this posterior.

Note that the naive same-distribution shortcut discussed in **Challenge 1** can be viewed as replacing this posterior with one that ignores the mask information, effectively treating missing values as if drawn from the observed-value distribution (e.g., $P(x | M = 0)$) rather than the MNAR-correct distribution for missing entries (e.g., $P(x | M = 1)$). Eq. (2) makes explicit that such a shortcut changes the integral measure and can bias the resulting predictive distribution.

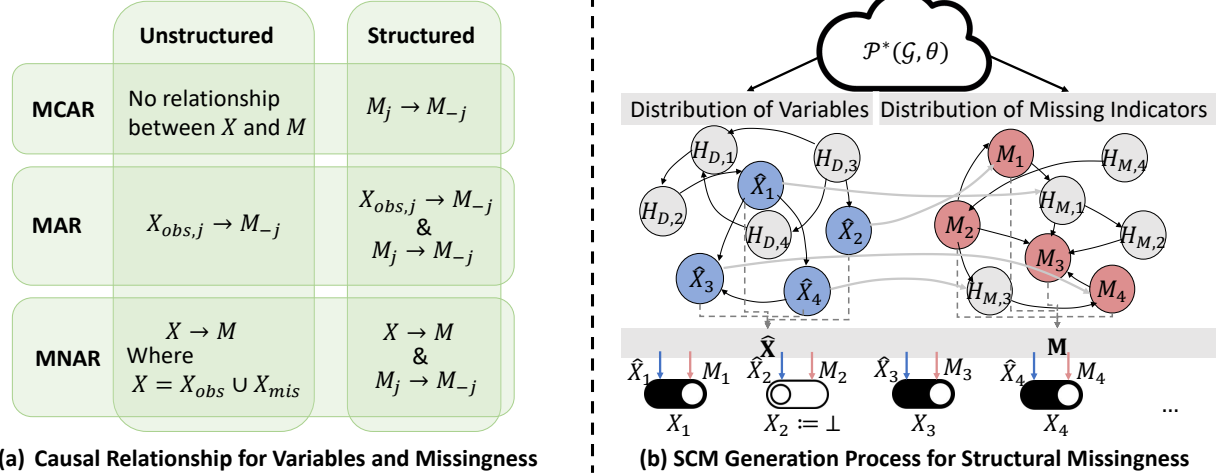


Figure 2. Second-order SCMs for structural missingness. **(Left)** A causal view of structural missingness, capturing both $X \rightarrow M$ (structural invalidity/undefined values) and $M \rightarrow M$ (missingness propagation) dependencies. **(Right)** The second-order SCM generation pipeline: sample a causal graph and parameters, generate complete data, then generate masks via the missingness mechanism; the resulting prior is used to fit PFNs and to learn the missing-value posterior.

However, making both parts tractable, and computing the required posterior predictive integral, is challenging. In the following sections, we derive a tractable approximation to the posterior by exploiting dependencies between observed and missing subspaces, and learn how to compose SCM-based data-generation and missingness mechanisms to better approximate the posterior predictive distribution.

4. Posterior Distribution of Structural Missingness

To model the structural missingness patterns, we employ second-order structural causal models (SCMs) (Figs. 1 and 2). This SCM defines the task prior whose induced posteriors we approximate: the observation channel $P(X_m^c | X_m)$ and the label map $P(y | X_m, D_m)$. PFNs amortize Bayes inference under this prior; if the prior is misspecified, the learned predictive is the best approximation within the model class in expected conditional KL (Theorem 6.1). The two fitting routes are introduced next in Sec. 5.

4.1. Causal Relationships for the Missing Indicators

Before formalizing the full generative model, we clarify the causal structure of the missingness indicators M . Let \mathbf{X} be the complete data matrix and \mathbf{M} the binary mask, where $M_{ij} = 1$ indicates that X_{ij} is missing. Classical settings distinguish MCAR/MAR/MNAR depending on whether M is independent of \mathbf{X} , depends on observed entries X_{obs} , or additionally depends on unobserved entries X_{miss} . In our scope, SM refers to structured (Markovian) dependence: the missingness mechanism (including the gate) is treated as a random variable under a second-order prior, while the

induced Markov structure of the SCM is fixed.

Importantly, missingness can also be *structured* within M itself (Fig. 2). The missingness of one field may force others to be missing, yielding edges $M_j \rightarrow M_{-j}$ (e.g., skipping “Smoker?” implies “Cigarettes per day” is undefined). Hence, a causal model for SM must capture both (1) $X \rightarrow M$ (state-dependent invalidity) and (2) $M \rightarrow M$ (propagation of missingness).

4.2. Constructing SCMs for Structural Missingness

We model SM with a Structural Causal Model (SCM) $\mathcal{M} = \langle \mathbf{X}, \mathbf{U}, \mathcal{F}, P(\mathbf{U}) \rangle$ and augment it with an explicit generator for the missingness mask \mathbf{M} . For each variable X_i , the missingness indicator is produced by $M_i \leftarrow f_{M_i}(PA(M_i), U_{M_i})$, where under SM, f_{M_i} is a deterministic gate that can depend on parent values ($X \rightarrow M$) and other indicators ($M \rightarrow M$). In our implementation we use a randomized score-and-quantile gate; details are in Appendix B. We further use a *second-order* SCM by treating the graph \mathcal{G} , parameters θ , and missingness logic as latent random variables. The resulting generative process is:

1. Sample a causal structure and parameters: $(\mathcal{G}, \theta) \sim P(\mathcal{G}, \theta)$.
2. Sample exogenous noise: $\mathbf{U} \sim P(\mathbf{U})$.
3. Generate complete data \mathbf{X} via structural equations $X_i \leftarrow f_i(PA_i, U_i)$.
4. Generate missingness indicators \mathbf{M} via $M_i \leftarrow f_{M_i}(PA(M_i))$, capturing both structural constraints ($X \rightarrow M$) and propagated missingness ($M \rightarrow M$).

5. Apply mask to obtain observed data: $X_{obs} = \mathbf{X} \odot (1 - \mathbf{M}) + \perp \odot \mathbf{M}$.

Our goal is the posterior induced by this SCM prior. In practice, we learn two prior-generated targets: the structural-missingness observation channel $P(X_m^c | X_m)$ and the label map $P(y | X_m, D_m)$, which motivates the two learned objects described next. See Appendix A to learn concretely about PFNs.

5. Fitting the PPDs and PDs for Structural Missingness

Given the decomposition in Eq. (2), our inference strategy requires estimating two key objects: the posterior predictive for labels, and (optionally) a posterior distribution (PD) over missing values. In this section, we detail our two-pronged approach: employing Prior Fitted Networks (PFNs) to learn $p(y | D_m^c, X_m^c)$ end-to-end from tasks generated by the SCM prior defined in Sec. 4, and utilizing Flow Matching as an auxiliary head to model the missing-value posterior conditioned on the same incomplete context.

5.1. Bayesian Inference with Prior Fitted Networks

Prior Fitted Networks (PFN) (Müller et al., 2022) are a class of neural networks designed to approximate Bayesian inference by learning a mapping from datasets to posterior predictive distributions (PPD). PFNs are trained on a large number of synthetic datasets generated from a prior distribution over models, allowing them to generalize to new datasets and perform inference efficiently.

In our framework, we treat the Second-Order SCM described in the previous section as the prior. A PFN, denoted as ϕ , is trained to approximate the posterior predictive distribution of the target label y given the observed data D_m^c and query X_m^c . Specifically, the PFN minimizes the cross-entropy loss between the predicted distribution and the true labels on synthetic tasks generated from the SCM prior:

$$\mathcal{L}_{PFN}(\phi) = \mathbb{E}_{(\mathcal{M}, D) \sim P(\mathcal{M}, D)} \left[- \sum_{(x, y) \in D_{test}} \log P_\phi(y | x, D_{train}) \right] \quad (3)$$

where (\mathcal{M}, D) is a dataset sampled from the second-order SCM prior. In our setting, the PFN consumes incomplete inputs (D_m^c, X_m^c) (including masks) and directly outputs the posterior predictive $p_\phi(y | D_m^c, X_m^c)$; the “general situation” is the special case with no missingness. This learned map implicitly marginalizes over latent missing values (and missing context D_m) under the SCM prior in a single forward pass.

5.2. Flow Matching Regressor for the PDs of Missing Variables

While the PFN already targets the required marginal posterior predictive $p_\phi(y | D_m^c, X_m^c)$ from incomplete data, we also learn a posterior over missing values for imputation and uncertainty analysis. Concretely, we train a Conditional Flow Matching (CFM) head to approximate $Q_\theta(X_m | X_m^c, D_m^c)$, where D_m is not represented explicitly but is marginalized through the same task prior that generates incomplete contexts. In contrast to MSE regression (which only learns a conditional mean), CFM can represent multimodal posteriors induced by structural constraints.

To address this, we propose using a **Flow Matching Regressor**. Inspired by Conformal Regression (Lei et al., 2018), our approach seeks to provide rigorous uncertainty quantification. However, unlike standard conformal methods which often focus on interval calibration, or MSE-based regressors that ignore the distributional shape, we aim to learn a *nearly KL-optimal* regression.

We employ Conditional Flow Matching (CFM) (Lipman et al., 2023) to learn a continuous normalizing flow that transforms a simple base distribution (e.g., Gaussian) into the complex posterior distribution of the missing variables conditioned on the observed ones. The objective is to minimize the regression loss between the vector field generated by the neural network $v_t(x, \theta)$ and the target vector field $u_t(x | x_1)$ defined by the probability path between the noise and data:

$$\mathcal{L}_{CFM}(\theta) = \mathbb{E}_{t, q(x_1), p_t(x | x_1)} \|v_t(x) - u_t(x | x_1)\|^2 \quad (4)$$

During pretraining, we balance this regression objective with the PFN cross-entropy using a fixed weight (CFM loss weight 0.1) and do not tune it extensively. The CFM head is conditioned on the same incomplete inputs (D_m^c, X_m^c, M) via the shared PFN-style backbone. In our pipeline, prediction does not require Monte Carlo over X_m or D_m : the PFN outputs $p_\phi(y | D_m^c, X_m^c)$ directly, while the flow head is used for explicit samples/imputations from Q_θ . Concrete pre-training hyperparameters (SCM prior distributions, missingness-generator settings, PFN backbone, and flow head) are provided in Appendix B.

6. Analysis of Bias Alleviation and Near Optimality During In-Context Learning

In this section we make precise near optimality in practice and why it is theoretically justified. The argument follows the subsection structure:

(1) *Risk minimization and approximation* establishes Bayes-near-optimality, with task-averaged training as an expected *conditional KL projection* (Theorem 6.1) and *consistency* for the missing-value posterior (Theorem 6.2). As properties

for methods in Secs. 4 & 5.

(2) *Bias alleviation* formalizes how posterior integration controls error via *posterior-mismatch* and *conditional prediction* terms (Theorem 6.3), explaining plug-in failures via the *Jensen gap* (Corollary 6.4) and unavoidable *MNAR mismatch* (Corollary 6.5, Remark 6.6). As previously introduced as **Challenges 1 & 3**.

and (3) *Sample complexity* for near-optimality, where the decoupled design is sufficiently non-biased and more *sample-efficient* than end-to-end learning (Theorem 6.7).

Notation. When the conditioning context (X_m^c, D_m^c) is clear, we abbreviate the true missing-value posterior and its learned approximation as

$$\mu := P^*(\cdot | X_m^c, D_m^c), \quad \nu := Q_\theta(\cdot | X_m^c, D_m^c).$$

With ϕ and θ denoting the PFN (predictive) and flow (posterior) parameters, respectively.

6.1. Risk Minimization and Approximation

To connect the model construction above with the bias and near-optimality results that follow, we first pin down what is learned in the population limit for the two components used in posterior integration.

How can we fit the posterior predictive distribution and the missing-value posterior nearly optimally, and when do these learned objects justify posterior integration?

In our instantiation, the posterior predictive is learned by a Prior-Fitted Network and the missing-value posterior is learned by conditional flow matching.

Theorem 6.1 (PFN as population risk minimization of posterior predictives). *Let Π be the second-order SCM prior over tasks (data-generating models). A task sampled from Π induces a random dataset D and, for any query x , a true posterior predictive distribution over labels $P^*(\cdot | x, D)$. Let $\{P_\phi(\cdot | x, D) : \phi \in \Phi\}$ be the PFN model class and consider the population cross-entropy risk*

$$\mathcal{R}(\phi) := \mathbb{E}_{(\mathcal{M}, D) \sim \Pi} \mathbb{E}_{x, y \sim P^*(\cdot, \cdot | D)} [-\log P_\phi(y | x, D)].$$

Then:

(i) *(Bayes optimality)* Any minimizer $\phi^* \in \arg \min_{\phi \in \Phi} \mathcal{R}(\phi)$ also minimizes the expected conditional KL divergence

$$\mathbb{E}_{(\mathcal{M}, D) \sim \Pi} \mathbb{E}_{x \sim P^*(\cdot | D)} [\text{KL}(P^*(\cdot | x, D) \| P_\phi(\cdot | x, D))],$$

and the minimum value equals the Bayes entropy term plus the minimum expected conditional KL.

- (ii) *(Realizable case)* If there exists $\bar{\phi} \in \Phi$ such that $P_{\bar{\phi}}(\cdot | x, D) = P^*(\cdot | x, D)$ for Π -almost every (x, D) , then any population risk minimizer satisfies $P_{\phi^*}(\cdot | x, D) = P^*(\cdot | x, D)$ Π -a.s.
- (iii) *(Misspecified case)* Without realizability, ϕ^* is the best approximation in Φ in the above expected conditional KL sense.

This is proved in the Appendix Sec. C.2.

Theorem 6.2 (Consistency of conditional flow matching in (Zhou & Liu, 2025)). *Let $P^*(X_m | X_m^c)$ be the true conditional distribution of missing variables. Under standard regularity conditions for conditional flow matching (existence/uniqueness of the probability path and sufficient model capacity), the population conditional flow matching objective is minimized when the learned conditional distribution equals the target, i.e., $Q_\theta(\cdot | X_m^c) = P^*(\cdot | X_m^c)$ almost surely in X_m^c . Moreover, with increasing data and a consistent optimizer, empirical minimizers converge to a population minimizer, yielding $Q_\theta(\cdot | X_m^c) \rightarrow P^*(\cdot | X_m^c)$ in an appropriate weak sense (e.g., W_1) under additional moment conditions.*

6.2. In-Model Reduction of Plug-in Imputation and MNAR Bias

To highlight the MNAR bias in **Challenge 1**, write $P(x | M = 0)$ and $P(x | M = 1)$ for the observed- and missing-value distributions. Under MNAR, $P(x | M = 1)$ can differ from $P(x | M = 0)$, so treating missingness as ignorable or using point imputation can introduce systematic bias. Our results show that posterior integration admits an explicit error bound (Theorem 6.3), point imputation can incur a strict Jensen gap (Corollary 6.4), and any imputer forced to use one distribution across missingness groups suffers unavoidable mismatch when $P(x | M = 1) \neq P(x | M = 0)$ (Corollary 6.5).

Let d be a metric on \mathcal{X}_m , and let W_1 be the 1-Wasserstein distance induced by d . The conditional complete-data target is written as $h^*(x_m) := \mathbb{E}[g(Y) | X_m = x_m, X_m^c, D_m^c]$ and the predictor is written as \hat{h}_ϕ (e.g., PFN).

Theorem 6.3 (Posterior integration converges with no in-model bias). *For any scalar test function g , define the true conditional target*

$$\begin{aligned} T_g^*(X_m^c, D_m^c) &:= \mathbb{E}[g(Y) | X_m^c, D_m^c] \\ &= \mathbb{E}_{X_m \sim \mu}[h^*(X_m)], \end{aligned} \tag{5}$$

and the posterior-integration estimator

$$\widehat{T}_g(X_m^c, D_m^c) := \mathbb{E}_{X_m \sim \nu}[\hat{h}_\phi(X_m)]. \tag{6}$$

Under Assumption C.1,

$$\left| T_g^*(X_m^c, D_m^c) - \widehat{T}_g(X_m^c, D_m^c) \right| \leq L \varepsilon_{post} + \varepsilon_{pred}. \quad (7)$$

This is proved in the Appendix Sec. C.3.

Corollary 6.4 (Strict Jensen gap of point imputation). *Let $\mu := P^*(\cdot \mid X_m^c, D_m^c)$ denote the true conditional distribution. If $h^*(\cdot)$ is strictly convex or strictly concave in x_m , μ is non-degenerate, and $\mathbb{E}_{X_m \sim \mu}[X_m]$ exists, then the point-imputation plug-in predictor*

$$\widehat{T}_{g,point} := h^*(\mathbb{E}_{X_m \sim \mu}[X_m]) \quad (8)$$

incurs a strict Jensen gap:

$$|\mathbb{E}_{X_m \sim \mu}[h^*(X_m)] - h^*(\mathbb{E}_{X_m \sim \mu}[X_m])| > 0. \quad (9)$$

This is proved in the Appendix Sec. C.4.

Corollary 6.5 (Inevitable mismatch under a forced same-distribution imputer). *Let P^* denote the true data-generating distribution, and define the conditional laws $P_0 := P^*(X_m \mid M = 0)$ and $P_1 := P^*(X_m \mid M = 1)$. Suppose $P_0 \neq P_1$ but an imputation/generative model is constrained to satisfy $R(X_m \mid M = 0) = R(X_m \mid M = 1) =: \tilde{P}$. Then no choice of \tilde{P} can match both P_0 and P_1 simultaneously; in particular,*

$$\max \{ \text{TV}(P_0, \tilde{P}), \text{TV}(P_1, \tilde{P}) \} \geq \frac{1}{2} \text{TV}(P_0, P_1). \quad (10)$$

Moreover, taking the supremum over bounded measurable f with $\|f\|_\infty \leq 1$,

$$\begin{aligned} \sup_{\|f\|_\infty \leq 1} \max \left\{ |\mathbb{E}_{P_0} f - \mathbb{E}_{\tilde{P}} f|, |\mathbb{E}_{P_1} f - \mathbb{E}_{\tilde{P}} f| \right\} \\ \geq \text{TV}(P_0, P_1), \end{aligned} \quad (11)$$

and hence at least one group ($M = 0$ or $M = 1$) incurs a non-vanishing distribution-mismatch bias whenever MNAR induces $P_0 \neq P_1$.

See Appendix Sec. C.5 for the proof.

Remark 6.6 (MNAR identifiability is model-dependent). Theorem 6.3 does not claim that MNAR is identifiable without assumptions. Rather, it formalizes an in-model inference statement: if the assumed SCM prior (including $X \rightarrow M$ and $M \rightarrow M$ structure) renders the posterior $P^*(X_m \mid X_m^c, D_m^c)$ identifiable within the model class, then learning that posterior and integrating it avoids systematic plug-in bias in prediction.

6.3. Sample Complexity Advantage of Decoupled Inference

The practical question is:

Given only the observed features x_m^c , and limited context D_m^c at test time, how can we predict y as close as possible to the Bayes-optimal answer?

Theorem 6.7 gives a sample-complexity advantage (ICL difficulty proxy) for learning G (missing-feature posterior) and H (conditional predictor) separately rather than end-to-end in finite-context / ICL. Appendix Sec. C.6 provides the supporting error decompositions and proof chain (Theorem C.9; Corollary C.10).

Theorem 6.7 (Sample Complexity Advantage of Decoupled Inference (ICL Difficulty Proxy)). *Consider the Bayes posterior-predictive target map $F(x_m^c, D_m^c) := P^*(\cdot \mid x_m^c, D_m^c)$. Equivalently, a “decoupled” view learns (i) a missing-feature posterior generator $G(\cdot \mid x_m^c, D_m^c) \approx P^*(\cdot \mid x_m^c, D_m^c)$ and (ii) a conditional predictor $H(\cdot \mid x_m, x_m^c, D_m^c) \approx P^*(\cdot \mid x_m, x_m^c, D_m^c)$, with the (conceptual) posterior-integrated predictor $\widehat{P}(y \mid x_m^c, D_m^c) := \int H(y \mid x_m, x_m^c, D_m^c) G(x_m \mid x_m^c, D_m^c) dx_m$.*

Assume the conditional predictor regularity in Appendix Sec. C.6 so that the posterior-mismatch term is controlled by $L_h W_1(\cdot, \cdot)$ (Lemma C.7). Then Corollary C.10 implies that to reach total error ϵ it suffices to learn G to Wasserstein accuracy $\epsilon/(2L_h)$ and H to conditional-prediction error $\epsilon/2$, capturing the required error propagation.

Further, using an effective complexity proxy viewpoint, assume learning a d -dimensional target to error ϵ scales as

$$\mathcal{N}(L, \epsilon) = \mathcal{O}((L/\epsilon)^d),$$

and let L_{cpl} denote an ICL coupling penalty (the added difficulty of learning the coupled posterior-integrated map directly from limited context). Then the end-to-end sample complexity \mathcal{N}_{E2E} versus the decoupled complexity $\mathcal{N}_{\text{Decoupled}}$ admits the comparison

$$\begin{aligned} \mathcal{N}_{E2E} &\approx \mathcal{O}\left(\left((L_h(1 + L_g) + L_{\text{cpl}})/\epsilon\right)^d\right), \\ \mathcal{N}_{\text{Decoupled}} &\approx \mathcal{O}\left(\left((L_g L_h)/\epsilon\right)^d\right) + \mathcal{O}\left(\left(L_h/\epsilon\right)^d\right), \end{aligned}$$

Thus, when L_g is large and context is limited (large L_{cpl}), learning G and H separately can be more sample-efficient than learning the coupled end-to-end map; see Appendix Sec. C.6.

7. Experiments

Details for Baselines and Benchmarks. Our evaluation is produced on 58 tabular datasets with missingness: for classification we report 33 datasets ($\leq 10\%$) + 10 datasets ($> 10\%$), covering 50 methods from 4 predictor families (XGBoost/LightGBM/CatBoost/TabPFN-family) and diverse missing-data handling. Dataset lists are in Appendix Tables 4–5 and full 50-method tables are in Appendix Tables 6–7. For imputation, we report MNAR robustness on $N = 15$ shared datasets with $K = 10$ masks (Appendix Table 3); protocol details are in Appendix Sec. B.1 and Sec. B.2.

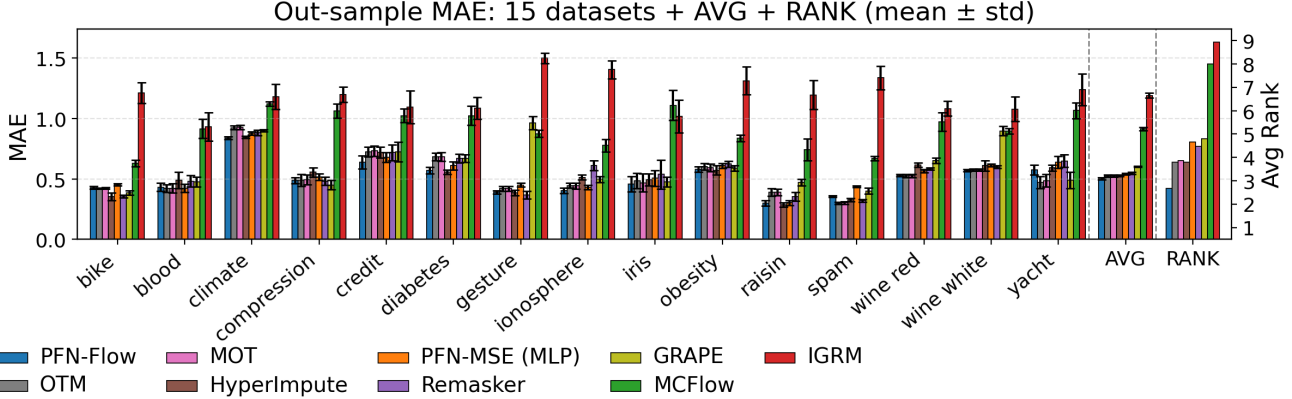


Figure 3. Out-of-sample MAE under MNAR (mean \pm std over $K = 10$ independently sampled MNAR mask realizations) across N datasets (here $N = 15$ from the cross-method intersection), with dataset-wise grouped bars, an aggregated AVG column, and an Avg Rank column on a secondary y-axis (lower is better).

Table 1. Method-level performance summary. Missing rate $\leq 10\%$. AUC is reported as mean \pm std across datasets. Rank denotes average per-dataset rank. Time is reported as mean \pm std(seconds) per 1000 instance with 50 variables. Datasets: 33. Showing top-14 + TabPFN (Raw) of 50 methods. Full results in Table 6.

Method	AUC	Rank	Time (s)
PFN-Flow	0.8694 ± 0.1448	16.83	0.061 ± 0.003
CatBoost + TDM	0.8664 ± 0.1512	20.77	160.830 ± 8.329
PFN-NSM	0.8663 ± 0.1499	18.70	0.061 ± 0.003
CatBoost + GRAPE	0.8660 ± 0.1521	21.65	43.530 ± 0.294
CatBoost + IGRM	0.8659 ± 0.1513	21.44	44.152 ± 0.241
CatBoost + OTM-SK	0.8657 ± 0.1514	20.70	82.744 ± 2.056
CatBoost + OTM-RR	0.8656 ± 0.1504	22.02	42.211 ± 0.211
CatBoost + Remasker	0.8656 ± 0.1501	21.32	551.288 ± 9.349
CatBoost + MOT-MLP	0.8646 ± 0.1527	22.94	165.097 ± 0.798
CatBoost + MCFlow	0.8646 ± 0.1522	20.91	65.533 ± 0.612
CatBoost + HyperImpute	0.8645 ± 0.1522	23.11	207.728 ± 0.543
CatBoost (Raw)	0.8642 ± 0.1523	22.17	37.031 ± 0.186
CatBoost + MissForest	0.8641 ± 0.1526	23.14	63.092 ± 1.692
CatBoost + MOT-LIN	0.8639 ± 0.1527	24.15	164.264 ± 3.783
TabPFN (Raw)	0.8545 ± 0.1610	26.73	0.061 ± 0.003

RQ1: Missing-data classification performance. **Question.** Which method is most accurate and robust across datasets under missingness? **Answer.** Tables 1 and 2 show that PFN-FLOW ranks first in both missingness regimes, outperforming TabPFN and PFN-NSM (an ablation using a reduced SCM prior as in Sec. 4.1: masks depend on X ($X \rightarrow M$) but have no cross-field propagation ($M \rightarrow M$)). This supports uncertainty-aware completion under structural missingness; see Appendix Sec. B.1.

RQ2: Missing-data classification efficiency. **Question.** How much runtime do we save relative to the strongest non-PFN baseline in the tables? **Answer.** We compute the speedup using the Time column in Tables 1 and 2 (baseline fit+inference, including fitting the imputer and classifier; PFN amortized forward-pass inference, with pre-training cost reported in Appendix Sec. B). In the low-missingness group, PFN-FLOW takes 0.061s while CatBoost+TDM takes 160.830s, giving a speedup of $160.830/0.061 \approx 2.6 \times 10^3$.

Table 2. Missing rate $> 10\%$. Datasets: 10. Showing top-14 + TabPFN (Raw) of 50 methods. Full results in Table 7.

Method	AUC	Rank	Time (s)
PFN-Flow	0.8172 ± 0.1099	11.40	0.061 ± 0.003
XGBoost + MOT-LIN	0.8111 ± 0.1217	12.00	131.921 ± 3.778
XGBoost + MOT-MLP	0.8073 ± 0.1216	17.60	132.754 ± 0.776
PFN-NSM	0.8065 ± 0.1219	16.20	0.061 ± 0.003
XGBoost + IGRM	0.8048 ± 0.1127	17.90	11.809 ± 0.156
XGBoost (Raw)	0.8047 ± 0.1117	15.50	4.689 ± 0.022
CatBoost + MOT-LIN	0.8042 ± 0.1228	22.40	164.264 ± 3.783
CatBoost + MOT-MLP	0.8039 ± 0.1249	20.30	165.097 ± 0.798
CatBoost (Raw)	0.8034 ± 0.1213	23.70	37.031 ± 0.186
XGBoost + GRAPE	0.8032 ± 0.1109	18.50	11.187 ± 0.229
XGBoost + OTM-RR	0.8028 ± 0.1206	21.40	9.869 ± 0.103
TabPFN + GRAPE	0.8016 ± 0.1301	24.90	6.560 ± 0.228
XGBoost + Remasker	0.8014 ± 0.1202	25.70	518.946 ± 9.348
TabPFN + MOT-LIN	0.8011 ± 0.1290	23.30	127.294 ± 3.778
TabPFN (Raw)	0.7985 ± 0.1269	23.50	0.061 ± 0.003

2.6×10^3 . In the high-missingness group, PFN-FLOW takes 0.061s while XGBoost+MOT-LIN takes 131.921s, giving $131.921/0.061 \approx 2.2 \times 10^3$. The runtime measurement protocol is detailed in Appendix Sec. B.1.

RQ3: MNAR imputation robustness. **Question.** Under MNAR missingness, do we improve out-of-sample imputation accuracy and consistency? **Answer.** Fig. 3 shows that PFN-FLOW achieves the lowest out-of-sample MAE and the best overall AVG and Avg Rank. The error bars are small, indicating consistent performance across MNAR masks (a practical robustness check without sweeping MNAR strength). The MNAR protocol and metrics are specified in Appendix Sec. B.2.

8. Conclusion

We propose near-optimal Bayesian inference under structural missingness. By casting the problem as a Second-

Order SCM and using Prior-Fitted Networks with Flow Matching, we obtain an approximation that preserves uncertainty rather than collapsing into a single imputation. Theory supports this view, and experiments show consistent gains over imputation baselines on incomplete tabular data.

Impact Statement

This paper presents work whose goal is to advance the field of Machine Learning. There are many potential societal consequences of our work, none which we feel must be specifically highlighted here.

References

Albergo, M., Boffi, N. M., and Vanden-Eijnden, E. Stochastic interpolants: A unifying framework for flows and diffusions. *Journal of Machine Learning Research*, 26(209):1–80, 2025.

Balazadeh, V., Kamkari, H., Thomas, V., Li, B., Ma, J., Cresswell, J. C., and Krishnan, R. G. CausalPFN: Amortized causal effect estimation via in-context learning. In *Advances in Neural Information Processing Systems*, volume 38, 2025. URL <https://github.com/vdblm/CausalPFN/>.

Chen, T. and Guestrin, C. Xgboost: A scalable tree boosting system. In Krishnapuram, B., Shah, M., Smola, A. J., Aggarwal, C. C., Shen, D., and Rastogi, R. (eds.), *Proceedings of the 22nd ACM SIGKDD International Conference on Knowledge Discovery and Data Mining, San Francisco, CA, USA, August 13-17, 2016*, pp. 785–794. ACM, 2016. doi: 10.1145/2939672.2939785. URL <https://doi.org/10.1145/2939672.2939785>.

Du, T., Melis, L., and Wang, T. Remasker: Imputing tabular data with masked autoencoding. In *The Twelfth International Conference on Learning Representations, ICLR 2024, Vienna, Austria, May 7-11, 2024*. OpenReview.net, 2024. URL <https://openreview.net/forum?id=K19NqjLVDT>.

García-Laencina, P. J., Sancho-Gómez, J.-L., and Figueiras-Vidal, A. R. Pattern classification with missing data: a review. *Neural Computing and Applications*, 19(2): 263–282, 2010.

Grinsztajn, L., Flöge, K., Key, O., Birkel, F., Jund, P., Roof, B., Jäger, B., Safaric, D., Alessi, S., Hayler, A., et al. TabPFN-2.5: Advancing the state of the art in tabular foundation models. *arXiv preprint arXiv:2511.08667*, 2025.

Hollmann, N., Müller, S., Eggensperger, K., and Hutter, F. TabPFN: A transformer that solves small tabular classification problems in a second. In *NeurIPS 2022 First Table Representation Workshop*, 2022.

Hollmann, N., Müller, S., Purucker, L., Krishnakumar, A., Körfer, M., Hoo, S. B., Schirrmeister, R. T., and Hutter, F. Accurate predictions on small data with a tabular foundation model. *Nat.*, 637(8044):319–326, 2025. doi: 10.1038/S41586-024-08328-6. URL <https://doi.org/10.1038/s41586-024-08328-6>.

Jarrett, D., Cebere, B., Liu, T., Curth, A., and van der Schaar, M. Hyperimpute: Generalized iterative imputation with automatic model selection. In Chaudhuri, K., Jegelka, S., Song, L., Szepesvári, C., Niu, G., and Sabato, S. (eds.), *International Conference on Machine Learning, ICML 2022, 17-23 July 2022, Baltimore, Maryland, USA*, volume 162 of *Proceedings of Machine Learning Research*, pp. 9916–9937. PMLR, 2022. URL <https://proceedings.mlr.press/v162/jarrett22a.html>.

Jolicoeur-Martineau, A., Fatras, K., and Kachman, T. Generating and imputing tabular data via diffusion and flow-based gradient-boosted trees. In *International conference on artificial intelligence and statistics*, pp. 1288–1296. PMLR, 2024.

Ke, G., Meng, Q., Finley, T., Wang, T., Chen, W., Ma, W., Ye, Q., and Liu, T. Lightgbm: A highly efficient gradient boosting decision tree. In Guyon, I., von Luxburg, U., Bengio, S., Wallach, H. M., Fergus, R., Vishwanathan, S. V. N., and Garnett, R. (eds.), *Advances in Neural Information Processing Systems 30: Annual Conference on Neural Information Processing Systems 2017, December 4-9, 2017, Long Beach, CA, USA*, pp. 3146–3154, 2017.

Kerrigan, G., Migliorini, G., and Smyth, P. Functional flow matching. *arXiv preprint arXiv:2305.17209*, 2023.

Lee, S., Kim, B., and Ye, J. C. Minimizing trajectory curvature of ode-based generative models. In *International Conference on Machine Learning*, pp. 18957–18973. PMLR, 2023.

Lei, J., G’Sell, M., Rinaldo, A., Tibshirani, R. J., and Wasserman, L. Distribution-free predictive inference for regression. *Journal of the American Statistical Association*, 113(523):1094–1111, 2018.

Lipman, Y., Chen, R. T. Q., Ben-Hamu, H., Nickel, M., and Le, M. Flow matching for generative modeling. In *The Eleventh International Conference on Learning Representations, ICLR 2023, Kigali, Rwanda, May 1-5, 2023*. OpenReview.net, 2023. URL <https://openreview.net/forum?id=PqvMRDCJT9t>.

Liu, S. and Ye, H. TabPFN unleashed: A scalable and effective solution to tabular classification problems. In *Forty-second International Conference on Machine Learning, ICML 2025, Vancouver, BC, Canada, July 13-19, 2025*.

OpenReview.net, 2025. URL <https://openreview.net/forum?id=5DD3RCcVcT>.

Ma, Z. and Chen, G. Bayesian methods for dealing with missing data problems. *Journal of the Korean Statistical Society*, 47(3):297–313, 2018.

Mitra, R., McGough, S. F., Chakraborti, T., Holmes, C. C., Copping, R., Hagenbuch, N., Biedermann, S., Noonan, J., Lehmann, B., Shenvi, A., Doan, X. V., Leslie, D., Bianconi, G., Sánchez-García, R. J., Davies, A. R., Mackintosh, M., Andrinopoulou, E., Basiri, A., Harbron, C., and MacArthur, B. D. Learning from data with structured missingness. *Nat. Mac. Intell.*, 5(1):13–23, 2023. doi: 10.1038/S42256-022-00596-Z. URL <https://doi.org/10.1038/s42256-022-00596-z>.

Mohan, K., Pearl, J., and Jin, T. Missing data as a causal inference problem. In *Proceedings of the neural information processing systems conference (nips)*, 2013.

Müller, S., Hollmann, N., Pineda-Arango, S., Grabocka, J., and Hutter, F. Transformers can do bayesian inference. In *The Tenth International Conference on Learning Representations, ICLR 2022, Virtual Event, April 25-29, 2022*. OpenReview.net, 2022. URL <https://openreview.net/forum?id=KSugKcbNf9>.

Müller, S., Feurer, M., Hollmann, N., and Hutter, F. Pfns4bo: In-context learning for bayesian optimization. In *International Conference on Machine Learning*, pp. 25444–25470. PMLR, 2023.

Müller, S. G., Reuter, A., Hollmann, N., Rügamer, D., and Hutter, F. The future of bayesian prediction is prior-fitted. In *Forty-second International Conference on Machine Learning, ICML 2025, Vancouver, BC, Canada, July 13–19, 2025*. OpenReview.net, 2025.

Muzellec, B., Josse, J., Boyer, C., and Cuturi, M. Missing data imputation using optimal transport. In *Proceedings of the 37th International Conference on Machine Learning, ICML 2020, 13–18 July 2020, Virtual Event*, volume 119 of *Proceedings of Machine Learning Research*, pp. 7130–7140. PMLR, 2020. URL <http://proceedings.mlr.press/v119/muzellec20a.html>.

Pearl, J. *Causality*. Cambridge university press, 2009.

Pereira, R. C., Abreu, P. H., and Rodrigues, P. P. Vaebridge: Variational autoencoder filter for bayesian ridge imputation of missing data. In *2020 International Joint Conference on Neural Networks (IJCNN)*, pp. 1–7. IEEE, 2020.

Pinkard, H. and Norlin, N. The missing data for intelligent scientific instruments. *Nature Methods*, pp. 1–4, 2025.

Prokhorenkova, L. O., Gusev, G., Vorobev, A., Dorogush, A. V., and Gulin, A. Catboost: unbiased boosting with categorical features. In Bengio, S., Wallach, H. M., Larochelle, H., Grauman, K., Cesa-Bianchi, N., and Garnett, R. (eds.), *Advances in Neural Information Processing Systems 31: Annual Conference on Neural Information Processing Systems 2018, NeurIPS 2018, December 3–8, 2018, Montréal, Canada*, pp. 6639–6649, 2018.

Pujianto, U., Wibawa, A. P., Akbar, M. I., et al. K-nearest neighbor (k-nn) based missing data imputation. In *2019 5th International Conference on Science in Information Technology (ICSITech)*, pp. 83–88. IEEE, 2019.

Qu, J., Holzmüller, D., Varoquaux, G., and Morvan, M. L. Tabicl: A tabular foundation model for in-context learning on large data. In *Forty-second International Conference on Machine Learning, ICML 2025, Vancouver, BC, Canada, July 13–19, 2025*. OpenReview.net, 2025. URL <https://openreview.net/forum?id=0VvD1PmNzM>.

Richardson, T. W., Wu, W., Lin, L., Xu, B., and Bernal, E. A. Mcflow: Monte carlo flow models for data imputation. In *2020 IEEE/CVF Conference on Computer Vision and Pattern Recognition, CVPR 2020, Seattle, WA, USA, June 13–19, 2020*, pp. 14193–14202. Computer Vision Foundation / IEEE, 2020. doi: 10.1109/CVPR42600.2020.01421.

Robertson, J., Reuter, A., Guo, S., Hollmann, N., Hutter, F., and Schölkopf, B. Do-PFN: In-context learning for causal effect estimation. In *Advances in Neural Information Processing Systems*, volume 38, 2025. URL <https://arxiv.org/abs/2506.03791>. Spotlight poster, NeurIPS 2025.

Rubin, D. B. Inference and missing data. *Biometrika*, 63(3): 581–592, 1976.

Rundel, D., Kobialka, J., von Crailsheim, C., Feurer, M., Nagerl, T., and Rügamer, D. Interpretable machine learning for tabPFN. In *World Conference on Explainable Artificial Intelligence*, pp. 465–476. Springer, 2024.

Spirites, P. and Glymour, C. An algorithm for fast recovery of sparse causal graphs. *Social science computer review*, 9(1):62–72, 1991.

Spirites, P., Glymour, C. N., and Scheines, R. *Causation, prediction, and search*. MIT press, 2000.

Stekhoven, D. J. and Bühlmann, P. Missforest - non-parametric missing value imputation for mixed-type data. *Bioinformatics*, 28 1:112–8, 2011. URL <https://api.semanticscholar.org/CorpusID:2089531>.

Vo, V., Zhao, H., Le, T., Bonilla, E. V., and Phung, D. Optimal transport for structure learning under missing data. In *Forty-first International Conference on Machine Learning, ICML 2024, Vienna, Austria, July 21-27, 2024*. OpenReview.net, 2024. URL <https://openreview.net/forum?id=09Robz3Ppy>.

Yoon, J., Jordon, J., and Schaar, M. Gain: Missing data imputation using generative adversarial nets. In *International conference on machine learning*, pp. 5689–5698. PMLR, 2018.

You, J., Ma, X., Ding, D. Y., Kochenderfer, M. J., and Leskovec, J. Handling missing data with graph representation learning. In Larochelle, H., Ranzato, M., Hadsell, R., Balcan, M., and Lin, H. (eds.), *Advances in Neural Information Processing Systems 33: Annual Conference on Neural Information Processing Systems 2020, NeurIPS 2020, December 6-12, 2020, virtual*, 2020.

Zhang, H., Fang, L., Wu, Q., and Yu, P. S. Diffputer: Empowering diffusion models for missing data imputation. In *The Thirteenth International Conference on Learning Representations, ICLR 2025, Singapore, April 24-28, 2025*. OpenReview.net, 2025. URL <https://openreview.net/forum?id=3f11SENSYO>.

Zhao, H., Sun, K., Dezfouli, A., and Bonilla, E. V. Transformed distribution matching for missing value imputation. In Krause, A., Brunskill, E., Cho, K., Engelhardt, B., Sabato, S., and Scarlett, J. (eds.), *International Conference on Machine Learning, ICML 2023, 23-29 July 2023, Honolulu, Hawaii, USA*, volume 202 of *Proceedings of Machine Learning Research*, pp. 42159–42186. PMLR, 2023. URL <https://proceedings.mlr.press/v202/zhao23h.html>.

Zhong, J., Gui, N., and Ye, W. Data imputation with iterative graph reconstruction. In Williams, B., Chen, Y., and Neville, J. (eds.), *Thirty-Seventh AAAI Conference on Artificial Intelligence, AAAI 2023, Thirty-Fifth Conference on Innovative Applications of Artificial Intelligence, IAAI 2023, Thirteenth Symposium on Educational Advances in Artificial Intelligence, EAAI 2023, Washington, DC, USA, February 7-14, 2023*, pp. 11399–11407. AAAI Press, 2023. doi: 10.1609/AAAI.V37I9.26348. URL <https://doi.org/10.1609/aaai.v37i9.26348>.

Zhou, Z. and Liu, W. An error analysis of flow matching for deep generative modeling. In *Forty-second International Conference on Machine Learning, ICML 2025, Vancouver, BC, Canada, July 13-19, 2025*. OpenReview.net, 2025. URL <https://openreview.net/forum?id=vES22INUKm>.

Appendix Contents

A Related Work	12
A.1 Structural Missingness	12
A.2 Prior-Fitted Networks	13
A.3 Generative Imputation	13
B Implementation Details	13
B.1 Missing Data Classification Experiments	15
B.2 Missing Data Imputation Experiments	15
C Theoretical Analysis	17
C.1 The Random Variables are Well-Defined	17
C.2 Proof of Theorem 6.1	17
C.3 Assumptions and Proof of Theorem 6.3	17
C.4 Proof of Corollary 6.4	18
C.5 Proof of Corollary 6.5	18
C.6 Posterior-Predictive Approximation via De-coupled Heads	19
C.7 Proof of Theorem 6.7	20
D Additional Experiments	21
D.1 Regression results under MCAR missingness	21
D.2 Boosting baselines	21
D.3 TabPFN variants and PFN-family baselines	21
D.4 Top split baselines	21

A. Related Work

A.1. Structural Missingness

While classic MCAR/MAR/ MNAR definitions (Rubin, 1976) cover probabilistic missingness, structural missingness deals with logically undefined values. Recent works have modeled this using graph-based approaches or separate categories, but often lack a unified Bayesian treatment. (Mohan et al., 2013) proposes and proved that dealing with missing data is a causal inference problem in a unified identification framework. However, due to lack of integration of methods and tools, models with simplified assumptions without considering selection bias caused by not explicitly differentiating $P(x|M = 0)$ and $P(x|M = 1)$ still dominate the field with plausible performance (Muzellec et al., 2020; Vo et al., 2024; Zhang et al., 2025). Though the structure is not identifiable in general without extra assumptions, PFNs can offer an “almost-free-lunch” in terms of *efficient amortized inference within an assumed SCM prior*: when the prior renders the relevant posteriors identifiable *in-model* (Remark 6.6), PFNs can approximate these posteriors and enable practical inference, rather than resolving fundamental MNAR non-identifiability without assumptions.

(Mitra et al., 2023) propose a comprehensive partition or break down of existing researches, which divides them into (1) making definitions for potential valuable/redundant parts and unignorable bias, such as (Rubin, 1976) first provide types that missing data can be classified into, (Muzellec et al., 2020) puts stress on types of missingness that cause unignorability bias.

The definitions provide a framework to (2) collect data and build models, such as KNN (Pujianto et al., 2019), Gaussian mixture based (García-Laencina et al., 2010), and Bayesian methods (Ma & Chen, 2018), for missing data imputation. Leveraging advanced mathematical frameworks that realize (1), (Muzellec et al., 2020; Vo et al., 2024) propose using optimal transport to measure the distance between the observed and missing data, and generative models such as (Zhang et al., 2025) propose using diffusion models to generate missing data.

The models provide tools to (3) make inference to find out truly valuable information to predict and make decisions with the models (Pinkard & Norlin, 2025), and most fundamentally (4) find physical rules and causal facts under general assumptions and minimal constraints (Pearl, 2009), which brings us back to (1) for constructing more effective modeling.

By considering this framework, we firstly find it more effective to construct missing mechanisms randomly, and fit a powerful regressor to make nearly Bayesian optimal inference on these missing data, which provides almost free lunch for merging the four parts of the loop in one inference.

A.2. Prior-Fitted Networks

PFNs (Müller et al., 2022; 2025) and TabPFN (Hollmann et al., 2022) demonstrate the power of learning Bayesian inference on tabular data. These methods have shown state-of-the-art performance on many small or medium-sized datasets since TabPFN-v2 (Hollmann et al., 2025). As concerns about scalability to larger datasets are raised, TabICL (Qu et al., 2025) proposes a distribution-aware feature embedding method to improve scalability, and BETA (Liu & Ye, 2025) adapts a lightweight encoder to align TabPFN to large-scale high-dimensional tabular data. As shown in the technical report for TabPFN-2.5 (Grinsztajn et al., 2025), it achieves dominant performance (87% win rate) on tabular datasets up to 100K samples and 2K features. PFN-based methods also have differentiable properties that can be leveraged to produce feature-importance measures, partial dependence (Rundel et al., 2024), and high-dimensional Bayesian optimization (Müller et al., 2023), and show promising results in settings requiring causal mechanisms, such as causal effect estimation (Balazadeh et al., 2025) and causal discovery (Robertson et al., 2025).

A.3. Generative Imputation

In tabular imputation, we aim to sample from a conditional distribution of missing entries given observed entries and a missingness mask, under heterogeneous feature types (continuous, discrete, categorical) and strong cross-feature constraints; in many practical settings this conditional mapping is close to deterministic (e.g., structurally constrained columns and rule-like relations).

Classical deep generative approaches for tabular completion include adversarial and VAE-style imputers such as GAIN (Yoon et al., 2018) and VAE-based models (Pereira et al., 2020), while more recent work leverages diffusion-style denoising for tabular imputation (e.g., Diffputer (Zhang et al., 2025)) and other modern generative formulations (Jolicoeur-Martineau et al., 2024).

Flow Matching (FM) (Lipman et al., 2023) provides an alternative ODE/SDE-based route: under the stochastic interpolant view, flows and diffusions can be unified (Albergro et al., 2025), but FM’s inductive bias is often better aligned with deterministic, physics-like constraints because it directly parameterizes a velocity field rather than a denoiser (Kerrigan et al., 2023). In addition, FM can learn near-straight transport paths related to optimal transport (Lipman et al., 2023), whereas diffusion trajectories are typically more curved; such curvature can amplify numerical integration error (Lee et al., 2023), making straighter paths particularly attractive for efficient, low-error deterministic imputation in tabular tasks.

B. Implementation Details

Implementation of the (Second-Order) SCM prior (abstract view). We model data generation using a (second-order) structural causal model (SCM). An SCM is a tuple $\mathcal{M} = \langle \mathbf{X}, \mathbf{U}, \mathcal{F}, P(\mathbf{U}) \rangle$, where $\mathbf{X} = (X_1, \dots, X_d)$ are endogenous variables, $\mathbf{U} = (U_1, \dots, U_d)$ are exogenous variables, and $\mathcal{F} = \{f_i\}_{i=1}^d$ are structural assignments. In a *second-order* SCM, we additionally randomize the causal graph \mathcal{G} (equivalently parent sets $\text{PA}(i)$) and the function parameters $\theta = \{\theta_i\}$, inducing a prior over mechanisms and structures.

Nodes (structural assignments). Each node X_i is generated by a structural equation

$$X_i \leftarrow f_i(X_{\text{PA}(i)}, U_i; \theta_i),$$

where $X_{\text{PA}(i)}$ denotes the vector of parent variables. We instantiate f_i as a depth- L feed-forward map (MLP) with elementwise nonlinearity ϕ :

$$\begin{aligned} h_i^{(0)} &= \Pi_i(X_{\text{PA}(i)}), \\ h_i^{(\ell)} &= \phi\left(W_i^{(\ell)} h_i^{(\ell-1)} + b_i^{(\ell)}\right) \quad (\ell = 1, \dots, L), \\ X_i &= g_i\left(h_i^{(L)}\right) + \sigma_i \varepsilon_i, \end{aligned}$$

where Π_i selects (and orders) the parent coordinates, and ε_i is a standardized noise term. This parameterization allows nonlinear, compositional effects along directed paths while keeping the SCM semantics explicit.

Edges (graph structure inside the parameterization). The directed edge $X_j \rightarrow X_i$ is represented by whether X_j is included in $\text{PA}(i)$ and, operationally, by whether the corresponding input-to-hidden connections in Π_i (or the first linear map) are active. Sampling a random graph prior can be implemented by randomly selecting parent sets and/or randomly sparsifying input connections (e.g., via independent masking of weights), which induces a distribution over adjacency patterns while keeping the functional form fixed. Nonlinearity ϕ governs how parent influences compose and interact, i.e., how edges combine beyond additive linear effects.

Exogenous variables (stochasticity and prior variability). Exogenous variables U_i are sampled i.i.d. from a simple base distribution (e.g., $U_i \sim \mathcal{N}(0, 1)$), and enter the model either (i) as explicit inputs to f_i or (ii) through an additive output noise term $\sigma_i \varepsilon_i$. Randomizing (\mathcal{G}, θ) further yields sample-to-sample mechanism variability, which is crucial for representing a rich prior over tabular-generating processes.

Table 3. Imputation benchmark datasets ($N = 15$ paper set). N : instances; D : features.

	bike	blood	climate	compression	credit	diabetes	gesture	ionosphere	iris	obesity	raisin	spam	wine red	wine white	yacht
N	8760	748	540	1030	690	442	9522	351	150	2111	900	4600	1599	4898	308
D	13	5	21	9	16	10	32	35	4	17	8	58	12	12	7

Table 4. Dataset summary for classification benchmarks. N : instances; D : features; Missing #: missing entries; Missing %: missing rate. low-missingness group (missing rate $\leq 10\%$).

Dataset	ID	N	D	Missing #	Missing %
Breast Cancer	13	286	9	9	0.35%
Breast W	15	699	10	16	0.23%
MUSHROOM	24	8124	23	2480	1.33%
Credit Approval	29	690	16	67	0.61%
Dermatology	35	366	35	8	0.06%
Sick	38	3772	30	6064	5.36%
Heart C	49	303	14	7	0.17%
Hepatitis	55	155	19	167	5.67%
Vote	56	435	16	392	5.63%
Lung Cancer	163	32	57	5	0.27%
Eucalyptus	188	736	20	448	3.04%
Cleveland	194	303	14	6	0.14%
Irish	451	500	6	32	1.07%
Analcatdata Broadwaymult	452	285	7	27	1.35%
Biomed	481	209	8	15	0.90%
Pharynx	738	195	10	2	0.10%
Cleveland	786	303	13	6	0.15%
Cholesterol	798	303	13	6	0.15%
Pbcseq	802	1945	18	1133	3.24%
AutoMpg	831	398	7	6	0.22%
Kdd El Nino Small	839	782	8	466	7.45%
AutoHorse	840	205	25	57	1.11%
BreastTumor	844	286	9	9	0.35%
Analcatdata Gsssexsurvey	852	159	9	6	0.42%
Chscase Whale	939	228	8	20	1.10%
Analcatdata Halloffame	966	1340	16	20	0.09%
Analcatdata Birthday	968	365	3	30	2.74%
Analcatdata Draft	984	366	4	1	0.07%
Cylinder Bands	6332	540	40	999	4.62%
SpeedDating	40536	8378	121	18372	1.81%
MiceProtein	40966	1080	82	1396	1.58%
DiabeticMellitus	41430	281	97	2	0.01%
Regime Alimentaire	42172	202	19	17	0.44%

Concrete prior instantiation (as used in our code). To make $P(\mathcal{G}, \theta)$ reproducible, we use a fixed generator family where each mechanism is a depth- L MLP with hidden width H and additive Gaussian noise. Mechanism diversity (and effective sparsity) is induced by randomly masking weights, optional block-wise sparsification, and random rotations/selection of observed coordinates from a shared latent representation; for causal tasks we enforce $H \geq d_y + 2d$ so that features, labels, and missingness scores can be sampled from the same representation. Exogenous causes are Gaussian, optionally with per-cause mean/scale randomization.

Prior over missingness mechanisms (randomized deterministic gates). We generate masks via a randomized score-and-quantile gate driven by a latent representation z (a concatenation of hidden states from the SCM generator). A score network g_ψ maps z to per-feature scores; to induce

Table 5. Dataset summary for classification benchmarks. N : instances; D : features; Missing #: missing entries; Missing %: missing rate. high-missingness group (missing rate $> 10\%$).

Dataset	ID	N	D	Missing #	Missing %
Labor		4	57	17	33.64%
Colic		25	368	26	20.14%
Colic		27	368	23	22.77%
Heart H		51	294	14	19.00%
Analcatdata Reviewer		460	379	7	48.13%
Pbc		524	418	20	1033
Pbc		810	418	18	1239
Colleges Usnews		930	1302	33	7830
Dresses Sales		23381	500	13	835
Titanic		42638	891	7	689

heterogeneity, we draw a layer index ℓ_j uniformly for each feature j and use the corresponding score s_{ij} . We then draw a per-feature quantile level $\alpha_j \sim \text{Unif}[\alpha_{\min}, \alpha_{\max}(t)]$, set the threshold τ_j to the empirical α_j -quantile of $\{s_{ij}\}_i$, and define $M_{ij} = 1[s_{ij} \leq \tau_j]$; label dimensions are always forced observed. In our default configuration, $\alpha_{\min} = 0.0$ and $\alpha_{\max}(t)$ is linearly warmed up from 0.3 to 0.8 over the first 1000 optimization steps.

Concrete pre-training details (for reproducibility). **SCM prior (graph and mechanisms).** Each synthetic task samples a nonlinear data-generating mechanism realized by a feed-forward network of depth $L \geq 2$, hidden width H , and an activation chosen from $\{\text{tanh}, \text{identity}, \text{ReLU}\}$. Mechanism diversity and effective graph sparsity are induced by (i) Bernoulli masking of weight matrices (with no masking in the first layer), (ii) optional block-wise sparsification, and (iii) random feature rotations and random selection/ordering of observed coordinates from a shared latent representation. Exogenous causes are sampled from a standard Gaussian, with optional per-cause mean/scale randomization; output noise is Gaussian with log-uniformly sampled scale. For classification tasks, we sample the number of classes uniformly from 2 to 10 and use a categorical-feature probability of 0.2.

Task size. We pre-train on tasks with feature dimension up to 100 and $n = 1152$ samples per task (with evaluation positions at $0.95n$).

Missingness logic. We use the score-and-quantile gate above, with a convolutional score network of two layers (kernel size 7) and tanh nonlinearity; missingness rates are controlled by $\alpha_{\min} = 0.0$ and a warmed-up $\alpha_{\max}(t)$ (from

0.3 to 0.8 over 1000 steps).

Model architectures. The PFN is a Transformer encoder with model width 512, 12 layers, 4 attention heads, feed-forward width 1024, dropout 0, and GELU activations; we embed both feature values and the binary mask and add them to form token embeddings. The conditional flow-matching head is a lightweight 2-layer Transformer that predicts the velocity field for masked entries using a sinusoidal time embedding; during training, the loss is computed only on masked entries, while the state is noisy everywhere.

Optimization. We train with Adam at learning rate 3×10^{-5} , cosine schedule with 20 warmup epochs and minimum learning rate 10^{-8} , no weight decay, and mixed precision; we also use a self-distillation auxiliary loss with weight 0.1. Synthetic tasks are generated on-the-fly from the prior; the default batch size is 64 tasks. For reference, we pre-train PFN-FLOW on a single NVIDIA RTX PRO 6000 GPU for 120 hours.

B.1. Missing Data Classification Experiments

Baselines. We compare strong, widely competitive tabular predictors, XGBOOST (Chen & Guestrin, 2016), LIGHTGBM (Ke et al., 2017), and CATBOOST (Prokhorenkova et al., 2018). We choose these baselines not merely because they are “standard”, but because they are consistently high-performing on real-world tabular benchmarks and remain strong when combined with mature missing-data pipelines. Concretely, we evaluate missing-data handling strategies spanning plug-in imputers such as MissForest (Stekhoven & Bühlmann, 2011), AutoML/statistical imputers such as HyperImpute (Jarrett et al., 2022), modern learned imputers including REMASKER (Du et al., 2024), GRAPE (You et al., 2020), IGRM (Zhong et al., 2023), MCFLOW (Richardson et al., 2020), and Transformed Distribution Matching (TDM) (Zhao et al., 2023), as well as OT-family methods including OT (Muzellec et al., 2020), OTM (Vo et al., 2024), and masked OT variants (MOT). For MOT, we report several practical variants that share the same OT-style objective but differ in the conditional model class used in the refinement step (e.g., linear vs. MLP), with a Sinkhorn-style OT baseline as a reference.

Dataset selection and benchmark name. To construct a reliable benchmark with real missingness, we filter OpenML tabular classification datasets using two simple rules: (i) the empirical missing rate is strictly positive (missing rate > 0), and (ii) the dataset falls within the practical operating range of TabPFN (e.g., feature dimensionality and sample size constraints for feasible inference). We call the resulting benchmark the *OpenML Missingness Benchmark (OMB)*.

We summarize the classification datasets in Tables 4 and 5, which are selected from OpenML and grouped by empirical

missing rate, including dataset size (N), inferred feature dimension (D), and missingness statistics (total missing entries and overall missing rate).

Full method tables (all methods). For the main paper (Sec. 7), we report a compact Top-15 summary for each missingness group in Tables 1 and 2. For completeness, we provide the corresponding full method summaries (all evaluated methods) in Tables 6 and 7 below. We report end-to-end wall-clock time per method as measured by our runtime benchmark. Concretely, for each method we measure the time to obtain predictions on a fixed $n = 1000, d = 50$ input, including fitting the imputer (if any) on the training split and applying it to train/test, plus fitting the classifier and running inference on the test split; PFN-family predictors require no target-dataset gradient training and are timed as amortized forward-pass inference.

B.2. Missing Data Imputation Experiments

Evaluation protocol. All methods are evaluated under exactly the same splits and masks through the unified baseline runners; for robustness, we report results on the intersection of datasets shared by all methods (here $N = 15$). We summarize the imputation benchmark datasets in Table 3 (dataset size N and feature dimension D).

Scalability to Larger Datasets. Empirically, the original TABPFN (Nature) recipe tends to dominate mainly in the small-data regime (roughly $N < 3,000$ instances), while follow-up lines such as TABICL and TABPFN-v2.5 introduce additional training/inference techniques that improve performance beyond that range and often dominate on larger datasets. Since our work does not adopt those large- N engineering tricks, we focus our imputation evaluation on real-world datasets with $N < 10,000$, which is sufficient for validating the missingness-inference component and the end-to-end uncertainty propagation studied in this paper.

Baselines. We compare against representative imputation baselines spanning masked autoencoding, graph-based reconstruction, generative flow models, and OT-based methods: REMASKER (Du et al., 2024), GRAPE (You et al., 2020), IGRM (Zhong et al., 2023), MCFLOW (Richardson et al., 2020), HYPERIMPUTE (Jarrett et al., 2022), MOT (Muzellec et al., 2020), and OTM (Vo et al., 2024).

MNAR logistic M2M (logistic MNAR with $M \rightarrow M$ propagation). Let $X \in \mathbb{R}^{n \times d}$ be the (fully observed) feature matrix before masking. We sample a subset of columns S as *logistic inputs* with $|S| = d_{in} = \max(\lfloor qd \rfloor, 1)$ (with $q = 0.3$ when $p \leq 0.3$ and $q = 0.1$ otherwise), and set $T = \{1, \dots, d\} \setminus S$. We first mask the input columns S independently with probability p (MCAR on S), yielding an

input mask $M_{i,S}$. Then for each $j \in T$, we draw the target mask using a logistic model that depends on both X and the already-sampled missingness in S :

$$P(M_{ij} = 1 | X, M_{i,S}) = \sigma((X_{i,S} \odot M_{i,S})^\top w_j + (1 - M_{i,S})^\top v_j + b_j), \quad (12)$$

where v_j linearly transforms the missingness indicators (thus capturing $M \rightarrow M$ propagation), and b_j is chosen (via bisection) to match the target missing rate p .

Table 6. Method-level AUC summary: mean/std, runtime, and average ranks. Missing rate $\leq 10\%$. AUC is reported as mean \pm std across datasets. **Rank** denotes the average per-dataset rank. **Time** is reported as mean \pm std(seconds) for time cost per 1000 instance with 50 variables. Datasets: 33. Showing all methods.

Method	AUC	Rank	Time (s)
PFN-Flow	0.8694 \pm 0.1448	16.83	0.061 \pm 0.003
CatBoost + TDM	0.8664 \pm 0.1512	20.77	160.830 \pm 8.329
PFN-NSM	0.8663 \pm 0.1499	18.70	0.061 \pm 0.003
CatBoost + GRAPE	0.8660 \pm 0.1521	21.65	43.530 \pm 0.294
CatBoost + IGRM	0.8659 \pm 0.1513	21.44	44.152 \pm 0.241
CatBoost + OTM-SK	0.8657 \pm 0.1514	20.70	82.744 \pm 2.056
CatBoost + OTM-RR	0.8656 \pm 0.1504	22.02	42.211 \pm 0.211
CatBoost + Remasker	0.8656 \pm 0.1501	21.32	551.288 \pm 9.349
CatBoost + MOT-MLP	0.8646 \pm 0.1527	22.94	165.097 \pm 0.798
CatBoost + MCFlow	0.8646 \pm 0.1522	20.91	65.533 \pm 0.612
CatBoost + HyperImpute	0.8645 \pm 0.1522	23.11	207.728 \pm 0.543
CatBoost (Raw)	0.8642 \pm 0.1523	22.17	37.031 \pm 0.186
CatBoost + MissForest	0.8641 \pm 0.1526	23.14	63.092 \pm 1.692
CatBoost + MOT-LIN	0.8639 \pm 0.1527	24.15	164.264 \pm 3.783
XGBoost + GRAPE	0.8638 \pm 0.1530	24.29	11.187 \pm 0.229
XGBoost + IGRM	0.8636 \pm 0.1531	23.48	11.809 \pm 0.156
XGBoost + MCFlow	0.8634 \pm 0.1523	22.80	33.190 \pm 0.584
XGBoost (Raw)	0.8634 \pm 0.1514	23.05	4.689 \pm 0.022
XGBoost + TDM	0.8633 \pm 0.1524	24.98	128.488 \pm 8.327
XGBoost + Remasker	0.8631 \pm 0.1513	24.92	518.946 \pm 9.348
XGBoost + OTM-SK	0.8627 \pm 0.1523	23.77	50.401 \pm 2.048
XGBoost + HyperImpute	0.8626 \pm 0.1523	25.12	175.385 \pm 0.510
XGBoost + MOT-MLP	0.8622 \pm 0.1532	25.17	132.754 \pm 0.776
XGBoost + OTM-RR	0.8621 \pm 0.1522	27.15	9.869 \pm 0.103
XGBoost + MissForest	0.8614 \pm 0.1534	28.29	30.749 \pm 1.682
XGBoost + MOT-LIN	0.8611 \pm 0.1536	26.62	131.921 \pm 3.778
LightGBM + GRAPE	0.8576 \pm 0.1585	25.88	14.986 \pm 0.240
TabPFN + MCFlow	0.8574 \pm 0.1592	26.33	28.563 \pm 0.583
LightGBM + TDM	0.8574 \pm 0.1585	27.44	132.287 \pm 8.328
TabPFN + Remasker	0.8574 \pm 0.1599	26.67	514.319 \pm 9.348
LightGBM + IGRM	0.8573 \pm 0.1584	26.47	15.608 \pm 0.172
TabPFN + HyperImpute	0.8571 \pm 0.1600	26.94	170.758 \pm 0.510
TabPFN + MOT-MLP	0.8571 \pm 0.1590	26.33	128.127 \pm 0.776
TabPFN + TDM	0.8570 \pm 0.1597	27.64	123.860 \pm 8.327
TabPFN + MissForest	0.8561 \pm 0.1613	27.64	26.122 \pm 1.681
LightGBM + Remasker	0.8559 \pm 0.1585	29.12	522.745 \pm 9.348
LightGBM + MCFlow	0.8557 \pm 0.1601	27.17	36.990 \pm 0.588
LightGBM + HyperImpute	0.8556 \pm 0.1589	29.09	179.184 \pm 0.515
LightGBM + OTM-RR	0.8556 \pm 0.1586	29.91	13.668 \pm 0.126
LightGBM + OTM-SK	0.8555 \pm 0.1596	28.27	54.200 \pm 2.049
TabPFN + OTM-SK	0.8554 \pm 0.1616	28.74	45.774 \pm 2.048
TabPFN + GRAPE	0.8547 \pm 0.1598	27.38	6.560 \pm 0.228
LightGBM + MOT-MLP	0.8545 \pm 0.1602	29.44	136.553 \pm 0.779
TabPFN (Raw)	0.8545 \pm 0.1610	26.73	0.061 \pm 0.003
LightGBM + MissForest	0.8541 \pm 0.1596	32.41	34.548 \pm 1.683
LightGBM (Raw)	0.8537 \pm 0.1626	28.74	8.488 \pm 0.075
LightGBM + MOT-LIN	0.8535 \pm 0.1609	30.79	135.721 \pm 3.779
TabPFN + OTM-RR	0.8532 \pm 0.1602	29.44	5.241 \pm 0.101
TabPFN + IGRM	0.8530 \pm 0.1593	27.71	7.182 \pm 0.154
TabPFN + MOT-LIN	0.8530 \pm 0.1580	29.24	127.294 \pm 3.778

Metric and aggregation (MAE, AVG, Avg Rank). We report *out-of-sample* MAE on the masked entries of the

test split (lower is better). For each dataset/method, we compute mean \pm std across the K MNAR mask realizations. To summarize performance across datasets, we report: (i) **AVG**: for each mask, we average MAE across the N datasets and then compute mean \pm std over the K masks; and (ii) **Avg Rank**: within each dataset, methods are ranked by their mask-averaged MAE (lower is better; ties receive average rank), and we average ranks across datasets. Avg Rank complements absolute MAE by emphasizing cross-dataset consistency under heterogeneous feature distributions and MNAR perturbations.

Table 7. Missing rate $> 10\%$. AUC is reported as mean \pm std across datasets. **Rank** denotes the average per-dataset rank. **Time** is reported as mean \pm std(seconds) for time cost per 1000 instance with 50 variables. Datasets: 10. Showing all methods.

Method	AUC	Rank	Time (s)
PFN-Flow	0.8172 \pm 0.1099	11.40	0.061 \pm 0.003
XGBoost + MOT-LIN	0.8111 \pm 0.1217	12.00	131.921 \pm 3.778
XGBoost + MOT-MLP	0.8073 \pm 0.1216	17.60	132.754 \pm 0.776
PFN-NSM	0.8065 \pm 0.1219	16.20	0.061 \pm 0.003
XGBoost + IGRM	0.8048 \pm 0.1127	17.90	11.809 \pm 0.156
XGBoost (Raw)	0.8047 \pm 0.1117	15.50	4.689 \pm 0.022
CatBoost + MOT-LIN	0.8042 \pm 0.1228	22.40	164.264 \pm 3.783
CatBoost + MOT-MLP	0.8039 \pm 0.1249	20.30	165.097 \pm 0.798
CatBoost (Raw)	0.8034 \pm 0.1213	23.70	37.031 \pm 0.186
XGBoost + GRAPE	0.8032 \pm 0.1109	18.50	11.187 \pm 0.229
XGBoost + OTM-RR	0.8028 \pm 0.1206	21.40	9.869 \pm 0.103
TabPFN + GRAPE	0.8016 \pm 0.1301	24.90	6.560 \pm 0.228
XGBoost + Remasker	0.8014 \pm 0.1202	25.70	518.946 \pm 9.348
TabPFN + MOT-LIN	0.8011 \pm 0.1290	23.30	127.294 \pm 3.778
TabPFN + MOT-MLP	0.8006 \pm 0.1311	23.50	128.127 \pm 0.776
TabPFN + TDM	0.8006 \pm 0.1294	24.80	123.860 \pm 8.327
CatBoost + Remasker	0.8005 \pm 0.1298	27.80	551.288 \pm 9.349
TabPFN + IGRM	0.8004 \pm 0.1283	24.90	7.182 \pm 0.154
TabPFN + MissForest	0.8002 \pm 0.1272	23.20	26.122 \pm 1.681
TabPFN + HyperImpute	0.8001 \pm 0.1285	23.10	170.758 \pm 0.510
XGBoost + OTM-SK	0.8000 \pm 0.1118	26.90	50.401 \pm 2.048
CatBoost + OTM-SK	0.8000 \pm 0.1180	26.10	82.744 \pm 2.056
TabPFN + Remasker	0.7998 \pm 0.1299	26.40	514.319 \pm 9.348
CatBoost + GRAPE	0.7997 \pm 0.1188	26.50	43.530 \pm 0.294
XGBoost + MissForest	0.7992 \pm 0.1190	22.10	30.749 \pm 1.682
CatBoost + IGRM	0.7986 \pm 0.1155	25.40	44.152 \pm 0.241
TabPFN (Raw)	0.7985 \pm 0.1269	23.50	0.061 \pm 0.003
TabPFN + MCFlow	0.7983 \pm 0.1214	25.80	28.563 \pm 0.583
XGBoost + HyperImpute	0.7982 \pm 0.1281	23.50	175.385 \pm 0.510
TabPFN + OTM-RR	0.7972 \pm 0.1272	28.20	5.241 \pm 0.101
CatBoost + TDM	0.7970 \pm 0.1187	28.90	160.830 \pm 8.329
XGBoost + TDM	0.7970 \pm 0.1141	26.40	128.488 \pm 8.327
CatBoost + HyperImpute	0.7964 \pm 0.1331	28.20	207.728 \pm 0.543
TabPFN + OTM-SK	0.7955 \pm 0.1315	28.90	45.774 \pm 2.048
CatBoost + MissForest	0.7947 \pm 0.1236	29.40	63.092 \pm 1.692
CatBoost + OTM-RR	0.7945 \pm 0.1253	31.70	42.211 \pm 0.211
XGBoost + MCFlow	0.7935 \pm 0.1187	21.40	33.190 \pm 0.584
CatBoost + MCFlow	0.7901 \pm 0.1161	25.20	65.533 \pm 0.612
LightGBM + MOT-LIN	0.7574 \pm 0.1384	26.85	135.721 \pm 3.779
LightGBM (Raw)	0.7565 \pm 0.1364	26.25	8.488 \pm 0.075
LightGBM + GRAPE	0.7561 \pm 0.1351	27.65	14.986 \pm 0.240
LightGBM + IGRM	0.7549 \pm 0.1345	27.75	15.608 \pm 0.172
LightGBM + MOT-MLP	0.7537 \pm 0.1363	30.55	136.553 \pm 0.779
LightGBM + OTM-RR	0.7523 \pm 0.1374	33.35	13.668 \pm 0.126
LightGBM + MCFlow	0.7509 \pm 0.1409	29.35	36.990 \pm 0.588
LightGBM + MissForest	0.7505 \pm 0.1337	33.65	34.548 \pm 1.683
LightGBM + TDM	0.7480 \pm 0.1336	36.85	132.287 \pm 8.328
LightGBM + Remasker	0.7477 \pm 0.1338	37.55	522.745 \pm 9.348
LightGBM + HyperImpute	0.7477 \pm 0.1383	34.35	179.184 \pm 0.515
LightGBM + OTM-SK	0.7472 \pm 0.1297	38.25	54.200 \pm 2.049

Protocol (data split + repeated MNAR masks). We follow the DiffPutter preprocessing pipeline: each dataset is

split into train/test with a 70/30 ratio. On the test split, we generate $K = 10$ independently sampled MNAR masks with missing rate $p = 0.3$, using the MNAR logistic mechanism `MNAR_logistic_M2M`.

C. Theoretical Analysis

C.1. The Random Variables are Well-Defined

Theorem: The objects X_m and X_m^c , defined as projections dependent on a random mask M , are well-defined random variables (measurable functions).

Proof. Let (Ω, \mathcal{F}, P) be the underlying probability space. Let $\mathbf{X} : \Omega \rightarrow \mathbb{R}^d$ and $M : \Omega \rightarrow \{0, 1\}^d$ be random variables. Let $S = \{0, 1\}^d$ denote the finite set of all possible masks.

To establish that X_m is a well-defined random variable, we must define a measurable space for its codomain. Since the dimension of X_m depends on M , the codomain is the disjoint union space $\mathbb{V} = \bigsqcup_{m \in S} \mathbb{R}^{|m|}$, equipped with the σ -algebra generated by the Borel sets on each component. For any measurable set $B \subseteq \mathbb{V}$, the preimage is:

$$X_m^{-1}(B) = \bigcup_{m \in S} \{\omega \in \Omega \mid M(\omega) = m\} \cap \{\omega \in \Omega \mid \text{Proj}(m, \mathbf{X}(\omega)) \in B \cap \mathbb{R}^{|m|}\}. \quad (13)$$

For a fixed m , the projection $\text{Proj}(m, \cdot)$ is a continuous linear map, making $\text{Proj}(m, \mathbf{X})$ a random variable. Thus, the second set in the intersection is in \mathcal{F} . Since M is a random variable, $\{M = m\} \in \mathcal{F}$. As \mathcal{F} is closed under finite intersections and unions, $X_m^{-1}(B) \in \mathcal{F}$, proving X_m is measurable.

Similarly, X_m^c maps to the product space $\mathbb{V}^c \times S$, where $\mathbb{V}^c = \bigsqcup_{m \in S} \mathbb{R}^{d-|m|}$. For any measurable set $C \times D \subseteq \mathbb{V}^c \times S$, the preimage decomposes as:

$$(X_m^c)^{-1}(C \times D) = \bigcup_{m \in D} \{\omega \in \Omega \mid M(\omega) = m\} \cap \{\omega \in \Omega \mid \text{Proj}(m^c, \mathbf{X}(\omega)) \in C \cap \mathbb{R}^{d-|m|}\}. \quad (14)$$

By the same logic, each term in the union is measurable. Therefore, X_m^c is a well-defined random variable. \square

C.2. Proof of Theorem 6.1

Proof. Fix (\mathcal{M}, D) and x . For any $R(\cdot)$ on labels,

$$\begin{aligned} & \mathbb{E}_{y \sim P^*(\cdot \mid x, D)}[-\log R(y)] \\ &= H(P^*(\cdot \mid x, D)) + \text{KL}(P^*(\cdot \mid x, D) \parallel R(\cdot)), \end{aligned}$$

where $H(\cdot)$ is Shannon entropy. Taking $R(\cdot) = P_\phi(\cdot \mid x, D)$ and averaging over (x, y, D) under Π yields

$$\begin{aligned} & \mathcal{R}(\phi) \\ &= \mathbb{E}_{(\mathcal{M}, D) \sim \Pi} \mathbb{E}_{x \sim P^*(\cdot \mid D)} \left[H(P^*(\cdot \mid x, D)) \right] + \\ & \quad \mathbb{E}_{(\mathcal{M}, D) \sim \Pi} \mathbb{E}_{x \sim P^*(\cdot \mid D)} \left[\text{KL}(P^*(\cdot \mid x, D) \parallel P_\phi(\cdot \mid x, D)) \right]. \end{aligned}$$

The first term is independent of ϕ , hence any minimizer of $\mathcal{R}(\phi)$ also minimizes the expected conditional KL, proving (i). If the minimum expected KL is zero (realizability), then any minimizer must satisfy $\text{KL}(P^* \parallel P_{\phi^*}) = 0$ Π -a.s., hence $P_{\phi^*} = P^*$ Π -a.s., proving (ii). Statement (iii) is immediate from (i). \square

C.3. Assumptions and Proof of Theorem 6.3

Assumption C.1 (Posterior approximation and predictor regularity). We assume:

- (A0) μ and ν have finite first moments under d (so W_1 is well-defined).
- (A1) The conditional complete-data target $h^*(x_m) := \mathbb{E}[g(Y) \mid X_m = x_m, X_m^c, D_m^c]$ is L -Lipschitz in x_m under d .
- (A2) The posterior approximation satisfies $W_1(\mu, \nu) \leq \varepsilon_{\text{post}}$.
- (A3) A predictor \hat{h}_ϕ (e.g., PFN) satisfies an integrated error bound under ν : $\left| \mathbb{E}_{X_m \sim \nu} [\hat{h}_\phi(X_m) - h^*(X_m)] \right| \leq \varepsilon_{\text{pred}}$.

We provide a fully detailed proof of Theorem 6.3. Throughout this section, we fix (X_m^c, D_m^c) and use the shorthand $\mu := P^*(\cdot \mid X_m^c, D_m^c)$ and $\nu := Q_\theta(\cdot \mid X_m^c, D_m^c)$ introduced in Assumption C.1.

Lemma C.2 (Tower property representation). *Let $h^*(x_m) := \mathbb{E}[g(Y) \mid X_m = x_m, X_m^c, D_m^c]$. Then*

$$\begin{aligned} T_g^*(X_m^c, D_m^c) &= \mathbb{E}[g(Y) \mid X_m^c, D_m^c] \\ &= \mathbb{E}_{X_m \sim \mu} [h^*(X_m)]. \end{aligned}$$

Proof. By the tower property of conditional expectation,

$$\begin{aligned} T_g^*(X_m^c, D_m^c) &= \mathbb{E}[g(Y) \mid X_m^c, D_m^c] \\ &= \mathbb{E}[\mathbb{E}[g(Y) \mid X_m, X_m^c, D_m^c] \mid X_m^c, D_m^c]. \end{aligned}$$

The inner conditional expectation equals $h^*(X_m)$ by definition, and under the conditioning (X_m^c, D_m^c) the random variable X_m is distributed as μ , hence the result. \square

Lemma C.3 (Error decomposition). *With $\widehat{T}_g(X_m^c, D_m^c) := \mathbb{E}_{X_m \sim \nu}[\widehat{h}_\phi(X_m)]$,*

$$|T_g^* - \widehat{T}_g| \leq |\mathbb{E}_\mu[h^*] - \mathbb{E}_\nu[h^*]| + |\mathbb{E}_\nu[h^* - \widehat{h}_\phi]|.$$

Proof. By Lemma C.2, $T_g^* = \mathbb{E}_\mu[h^*(X_m)]$. Therefore,

$$\begin{aligned} |T_g^* - \widehat{T}_g| &= |\mathbb{E}_\mu[h^*(X_m)] - \mathbb{E}_\nu[\widehat{h}_\phi(X_m)]| \\ &\leq |\mathbb{E}_\mu[h^*] - \mathbb{E}_\nu[h^*]| + |\mathbb{E}_\nu[h^* - \widehat{h}_\phi]|, \end{aligned}$$

by adding and subtracting $\mathbb{E}_\nu[h^*(X_m)]$ and applying the triangle inequality. \square

Lemma C.4 (Lipschitz test functions and Wasserstein-1). *If h^* is L -Lipschitz under d and W_1 is induced by d , then*

$$|\mathbb{E}_\mu[h^*] - \mathbb{E}_\nu[h^*]| \leq L W_1(\mu, \nu).$$

Proof. Assumption C.1(A0) ensures $W_1(\mu, \nu)$ is well-defined. By Kantorovich–Rubinstein duality,

$$W_1(\mu, \nu) = \sup_{\text{Lip}(f) \leq 1} (\mathbb{E}_\mu[f] - \mathbb{E}_\nu[f]).$$

If h^* is L -Lipschitz, then $f := h^*/L$ is 1-Lipschitz when $L > 0$ (the claim is trivial if $L = 0$). Hence

$$\begin{aligned} |\mathbb{E}_\mu[h^*] - \mathbb{E}_\nu[h^*]| &= L |\mathbb{E}_\mu[f] - \mathbb{E}_\nu[f]| \\ &\leq L W_1(\mu, \nu). \end{aligned}$$

\square

Proof of Theorem 6.3. By Lemma C.3,

$$|T_g^* - \widehat{T}_g| \leq |\mathbb{E}_\mu[h^*] - \mathbb{E}_\nu[h^*]| + |\mathbb{E}_\nu[h^* - \widehat{h}_\phi]|.$$

The second term is bounded by Assumption C.1(A3), yielding $|\mathbb{E}_\nu[h^* - \widehat{h}_\phi]| \leq \varepsilon_{\text{pred}}$. For the first term, Lemma C.4 gives $|\mathbb{E}_\mu[h^*] - \mathbb{E}_\nu[h^*]| \leq L W_1(\mu, \nu)$, and Assumption C.1(A2) implies $W_1(\mu, \nu) \leq \varepsilon_{\text{post}}$. Combining yields

$$|T_g^* - \widehat{T}_g| \leq L \varepsilon_{\text{post}} + \varepsilon_{\text{pred}}.$$

\square

C.4. Proof of Corollary 6.4

Proof. Let $\mu := P^*(\cdot | X_m^c, D_m^c)$ as in the corollary statement. By assumption, h^* is strictly convex or strictly concave, μ is non-degenerate, and $\mathbb{E}_{X_m \sim \mu}[X_m]$ exists.

If h^* is strictly convex, then by the strict Jensen inequality,

$$\mathbb{E}_{X_m \sim \mu}[h^*(X_m)] > h^*(\mathbb{E}_{X_m \sim \mu}[X_m]).$$

If h^* is strictly concave, the inequality reverses. In either case, since μ is non-degenerate, the inequality is strict, yielding

$$|\mathbb{E}_{X_m \sim \mu}[h^*(X_m)] - h^*(\mathbb{E}_{X_m \sim \mu}[X_m])| > 0.$$

\square

C.5. Proof of Corollary 6.5

Proof. Recall the variational characterization

$$\text{TV}(P_0, P_1) = \sup_{\|f\|_\infty \leq 1} \frac{1}{2} |\mathbb{E}_{P_0} f - \mathbb{E}_{P_1} f|.$$

Let $\varepsilon > 0$ and choose f_ε with $\|f_\varepsilon\|_\infty \leq 1$ such that

$$\frac{1}{2} |\mathbb{E}_{P_0} f_\varepsilon - \mathbb{E}_{P_1} f_\varepsilon| \geq \text{TV}(P_0, P_1) - \varepsilon.$$

For any candidate \tilde{P} , the triangle inequality gives

$$\begin{aligned} |\mathbb{E}_{P_0} f_\varepsilon - \mathbb{E}_{P_1} f_\varepsilon| &\leq |\mathbb{E}_{P_0} f_\varepsilon - \mathbb{E}_{\tilde{P}} f_\varepsilon| + |\mathbb{E}_{\tilde{P}} f_\varepsilon - \mathbb{E}_{P_1} f_\varepsilon| \\ &\leq 2 \max \{ |\mathbb{E}_{P_0} f_\varepsilon - \mathbb{E}_{\tilde{P}} f_\varepsilon|, |\mathbb{E}_{P_1} f_\varepsilon - \mathbb{E}_{\tilde{P}} f_\varepsilon| \}, \end{aligned}$$

which implies

$$\max \{ |\mathbb{E}_{P_0} f_\varepsilon - \mathbb{E}_{\tilde{P}} f_\varepsilon|, |\mathbb{E}_{P_1} f_\varepsilon - \mathbb{E}_{\tilde{P}} f_\varepsilon| \} \geq \text{TV}(P_0, P_1) - \varepsilon.$$

Since $\varepsilon > 0$ is arbitrary, taking the supremum over $\|f\|_\infty \leq 1$ yields

$$\sup_{\|f\|_\infty \leq 1} \max \{ |\mathbb{E}_{P_0} f - \mathbb{E}_{\tilde{P}} f|, |\mathbb{E}_{P_1} f - \mathbb{E}_{\tilde{P}} f| \} \geq \text{TV}(P_0, P_1).$$

Finally, using the variational characterization (for any distributions R, S),

$$\sup_{\|f\|_\infty \leq 1} |\mathbb{E}_R f - \mathbb{E}_S f| = 2 \text{TV}(R, S)$$

and applying it with $(R, S) = (P_0, \tilde{P})$ and (P_1, \tilde{P}) gives

$$\begin{aligned} \max \{ \sup_{\|f\|_\infty \leq 1} |\mathbb{E}_{P_0} f - \mathbb{E}_{\tilde{P}} f|, \sup_{\|f\|_\infty \leq 1} |\mathbb{E}_{P_1} f - \mathbb{E}_{\tilde{P}} f| \} \\ = 2 \max \{ \text{TV}(P_0, \tilde{P}), \text{TV}(P_1, \tilde{P}) \}. \end{aligned}$$

Since $\max \{ \sup a_f, \sup b_f \} \geq \sup \max \{ a_f, b_f \}$, combining with the previous inequality yields

$$\max \{ \text{TV}(P_0, \tilde{P}), \text{TV}(P_1, \tilde{P}) \} \geq \frac{1}{2} \text{TV}(P_0, P_1)$$

\square

C.6. Posterior-Predictive Approximation via Decoupled Heads

The Bayes posterior predictive integrates over the posterior of missing features, conditional on the observed features and the available context data. In our implementation, the PFN head is trained to *directly* output the marginalized posterior predictive $P_\phi(\cdot | x_m^c, D_m^c)$ from incomplete contexts (implicit marginalization), while the flow head optionally learns an explicit missing-value posterior $Q_\theta(x_m | x_m^c, D_m^c)$ for sampling/imputation and uncertainty analysis. The lemmas below provide a proof chain that (i) characterizes posterior integration as a marginalization identity, (ii) decomposes decoupled approximation error into posterior-mismatch and conditional-prediction terms, (iii) controls posterior mismatch by a W_1 distance under Lipschitz regularity, and (iv) links PFN-style conditional KL training to bounded test-function error via total variation and Pinsker's inequality.

Lemma C.5 (Posterior-predictive marginalization). *Let D_m^c denote the context data available at test time, and let x_m^c and x_m be the observed and missing parts of x , respectively. Assuming the conditional distributions are well-defined, the Bayes posterior predictive satisfies*

$$\begin{aligned} P^*(y | x_m^c, D_m^c) \\ = \int P^*(y | x_m, x_m^c, D_m^c) P^*(x_m | x_m^c, D_m^c) dx_m. \end{aligned}$$

Proof. This is the law of total probability (or iterated expectation) applied to the latent missing features x_m :

$$\begin{aligned} P^*(y | x_m^c, D_m^c) \\ = \int P^*(y, x_m | x_m^c, D_m^c) dx_m \\ = \int P^*(y | x_m, x_m^c, D_m^c) P^*(x_m | x_m^c, D_m^c) dx_m. \end{aligned}$$

□

Lemma C.6 (Decoupled approximation error decomposition). *Fix (x_m^c, D_m^c) . Let G be a posterior generator that induces a distribution $G(\cdot | x_m^c, D_m^c)$ over x_m , and let $H(\cdot | x_m, x_m^c, D_m^c)$ be a conditional predictor (e.g., a classifier). Define the induced posterior-predictive mixture*

$$\begin{aligned} \hat{P}(y | x_m^c, D_m^c) \\ := \int H(y | x_m, x_m^c, D_m^c) G(x_m | x_m^c, D_m^c) dx_m. \end{aligned}$$

Then, for any measurable function φ with $\|\varphi\|_\infty \leq 1$,

$$\begin{aligned} |\mathbb{E}_{\hat{P}}[\varphi(y)] - \mathbb{E}_{P^*}[\varphi(y)]| \leq \\ \underbrace{|\mathbb{E}_{x_m \sim G} \mathbb{E}_{y \sim H}[\varphi(y)] - \mathbb{E}_{x_m \sim P^*(\cdot | x_m^c, D_m^c)} \mathbb{E}_{y \sim H}[\varphi(y)]|}_{\text{posterior approximation (learn } G\text{)}} + \\ \underbrace{\left| \mathbb{E}_{x_m \sim P^*(\cdot | x_m^c, D_m^c)} \left| \frac{\mathbb{E}_{y \sim H}[\varphi(y)] - \mathbb{E}_{y \sim P^*(\cdot | x_m, x_m^c, D_m^c)}[\varphi(y)]}{\mathbb{E}_{y \sim P^*(\cdot | x_m, x_m^c, D_m^c)}[\varphi(y)]} \right| \right|}_{\text{conditional prediction (learn } H\text{)}}. \end{aligned}$$

Proof. By definition of \hat{P} ,

$$\mathbb{E}_{\hat{P}}[\varphi(y)] = \mathbb{E}_{x_m \sim G(\cdot | x_m^c, D_m^c)} \mathbb{E}_{y \sim H(\cdot | x_m, x_m^c, D_m^c)}[\varphi(y)].$$

Also, by Lemma C.5,

$$\mathbb{E}_{P^*}[\varphi(y)] = \mathbb{E}_{x_m \sim P^*(\cdot | x_m^c, D_m^c)} \mathbb{E}_{y \sim P^*(\cdot | x_m, x_m^c, D_m^c)}[\varphi(y)].$$

Add and subtract $\mathbb{E}_{x_m \sim P^*(\cdot | x_m^c, D_m^c)} \mathbb{E}_{y \sim H(\cdot | x_m, x_m^c, D_m^c)}[\varphi(y)]$ and apply the triangle inequality to obtain the stated bound. □

Lemma C.7 (Bounding posterior mismatch by W_1). *Assume that for fixed (x_m^c, D_m^c) and for any φ with $\|\varphi\|_\infty \leq 1$, the map $x_m \mapsto \mathbb{E}_{y \sim H(\cdot | x_m, x_m^c, D_m^c)}[\varphi(y)]$ is L_h -Lipschitz w.r.t. $\|\cdot\|_2$. Then the first term in Lemma C.6 is bounded by*

$$L_h W_1(G(\cdot | x_m^c, D_m^c), P^*(\cdot | x_m^c, D_m^c)),$$

where W_1 is the Wasserstein-1 distance.

Proof. Fix (x_m^c, D_m^c) and define

$$f(x_m) := \mathbb{E}_{y \sim H(\cdot | x_m, x_m^c, D_m^c)}[\varphi(y)].$$

By assumption, f is L_h -Lipschitz. By Kantorovich–Rubinstein duality,

$$\begin{aligned} |\mathbb{E}_{x_m \sim G} f(x_m) - \mathbb{E}_{x_m \sim P^*(\cdot | x_m^c, D_m^c)} f(x_m)| \\ \leq L_h W_1(G(\cdot | x_m^c, D_m^c), P^*(\cdot | x_m^c, D_m^c)), \end{aligned}$$

which is exactly the desired bound. □

Lemma C.8 (From conditional KL to bounded test functions (Pinsker)). *Fix (x_m^c, D_m^c) . Let $R := P^*(\cdot | x_m^c, D_m^c)$ and let S be any learned posterior predictive distribution over y (e.g., a PFN output $S := P_\phi(\cdot | x_m^c, D_m^c)$). Define total variation as $\text{TV}(R, S) := \sup_A |R(A) - S(A)|$. Then for any measurable φ with $\|\varphi\|_\infty \leq 1$,*

$$|\mathbb{E}_R[\varphi] - \mathbb{E}_S[\varphi]| \leq 2 \text{TV}(R, S) \leq \sqrt{2 \text{KL}(R \| S)}.$$

Proof. The first inequality follows from the variational characterization $\sup_{\|\varphi\|_\infty \leq 1} |\mathbb{E}_R \varphi - \mathbb{E}_S \varphi| = 2 \text{TV}(R, S)$ under the above convention for TV. The second inequality is Pinsker's inequality, $\text{TV}(R, S) \leq \sqrt{\frac{1}{2} \text{KL}(R \| S)}$. Combining the two bounds yields the claim. □

Proposition C.9 (Why decoupling helps approximate Bayes posterior predictive with limited context). *Under the identifiability condition in Remark 6.6 (so that $P^*(x_m | x_m^c, D_m^c)$ is well-defined within the model class), Lemmas C.6–C.7 show that approximating the Bayes posterior predictive reduces to separately learning (i) the posterior over missing features (G) and (ii) the conditional predictor (H). Moreover, Lemma C.8 shows how PFN-style training that minimizes conditional cross-entropy (equivalently, conditional KL in the realizable case) controls bounded test-function error for the marginalized posterior predictive without explicitly computing the integral in Lemma C.5. Combined with Theorem 6.7, this supports the claim that, with limited context (test-time training / in-context learning), a decoupled multi-task design can be more sample-efficient and thereby more favorable for approximating the Bayes-optimal posterior predictive than directly learning the coupled end-to-end map.*

Proof. Under Remark 6.6, the Bayes posterior predictive is well-defined in-model. Lemmas C.6–C.7 decompose the approximation error into (i) a posterior-mismatch term (bounded by a W_1 distance for G) and (ii) a conditional-prediction term for H . Hence, approximating the posterior predictive reduces to learning G and H to control these two terms. Lemma C.8 provides a direct route for the PFN head: small conditional KL to the true posterior predictive implies small bounded test-function error for the marginalized predictor. Theorem 6.7 adds a complementary complexity argument: when the structural component is highly nonlinear (large effective L_g) and context is limited (large coupling difficulty), learning the decoupled components can be more sample-efficient than learning the coupled end-to-end map in the ICL regime. \square

Corollary C.10 (Explicit link to complexity via a two-term target). *Under the assumptions of Lemmas C.6–C.7, for any φ with $\|\varphi\|_\infty \leq 1$,*

$$|\mathbb{E}_{\hat{P}}[\varphi(y)] - \mathbb{E}_{P^*}[\varphi(y)]| \leq L_h W_1(G(\cdot | x_m^c, D_m^c), P^*(\cdot | x_m^c, D_m^c)) + \epsilon_H(x_m^c, D_m^c),$$

where $\epsilon_H(x_m^c, D_m^c) := \mathbb{E}_{x_m \sim P^*(\cdot | x_m^c, D_m^c)} |\mathbb{E}_{y \sim H}[\varphi(y)] - \mathbb{E}_{y \sim P^*}[\varphi(y)]|$ is the conditional prediction error term. In particular, to ensure the total error is at most ϵ , it suffices to budget $W_1(G, P^*) \leq \epsilon/(2L_h)$ and $\epsilon_H(x_m^c, D_m^c) \leq \epsilon/2$, making the required error propagation through L_h explicit. Thus, approximating the posterior predictive can be viewed as a two-term learning target (learn G to reduce W_1 , learn H to reduce ϵ_H), aligning with Theorem 6.7 where the decoupled sample-complexity proxy depends on the effective complexities of G and H and the ICL coupling difficulty of learning the coupled map directly.

Proof. Apply Lemma C.6 and then upper bound the first (posterior approximation) term by Lemma C.7. The remaining term is exactly $\epsilon_H(x_m^c, D_m^c)$ by definition. \square

C.7. Proof of Theorem 6.7

Proof. We make explicit the proxy assumptions used by Theorem 6.7. Assume there exists a function $\mathcal{N}(L, \epsilon)$ such that, for a d -dimensional learning target with effective complexity parameter L , achieving error at most ϵ requires

$$\mathcal{N}(L, \epsilon) = \mathcal{O}((L/\epsilon)^d).$$

Define L_g as the effective complexity parameter governing the difficulty of learning the missing-feature posterior map $(x_m^c, D_m^c) \mapsto P^*(x_m | x_m^c, D_m^c)$ to Wasserstein-1 accuracy, and define $L_{\text{cpl}} \geq 0$ as an additional coupling penalty for learning the coupled end-to-end posterior-predictive map directly from limited context.

By Corollary C.10, to ensure total test-function error at most ϵ it suffices to satisfy

$$W_1(G(\cdot | x_m^c, D_m^c), P^*(\cdot | x_m^c, D_m^c)) \leq \frac{\epsilon}{2L_h}$$

and

$$\epsilon_H(x_m^c, D_m^c) \leq \frac{\epsilon}{2}.$$

Under the proxy sample-complexity law, learning G to Wasserstein error $\epsilon/(2L_h)$ requires at most

$$\mathcal{N}\left(L_g, \frac{\epsilon}{2L_h}\right) = \mathcal{O}\left((L_g L_h)/\epsilon\right)^d,$$

and learning H to conditional-prediction error $\epsilon/2$ requires at most

$$\mathcal{N}\left(L_h, \frac{\epsilon}{2}\right) = \mathcal{O}\left((L_h/\epsilon)^d\right),$$

where constant factors are absorbed into $\mathcal{O}(\cdot)$. Summing the two requirements yields

$$\mathcal{N}_{\text{Decoupled}} \approx \mathcal{O}\left((L_g L_h)/\epsilon\right)^d + \mathcal{O}\left((L_h/\epsilon)^d\right).$$

For the coupled end-to-end predictor, apply the same proxy law to the d -dimensional target map $F(x_m^c, D_m^c) = P^*(\cdot | x_m^c, D_m^c)$, and assume its effective complexity is upper bounded (up to constants) by $L_h(1 + L_g) + L_{\text{cpl}}$. Then achieving error at most ϵ requires

$$\begin{aligned} \mathcal{N}_{\text{E2E}} &\approx \mathcal{N}(L_h(1 + L_g) + L_{\text{cpl}}, \epsilon) \\ &= \mathcal{O}\left((L_h(1 + L_g) + L_{\text{cpl}})/\epsilon\right)^d, \end{aligned}$$

which is exactly the stated comparison. \square

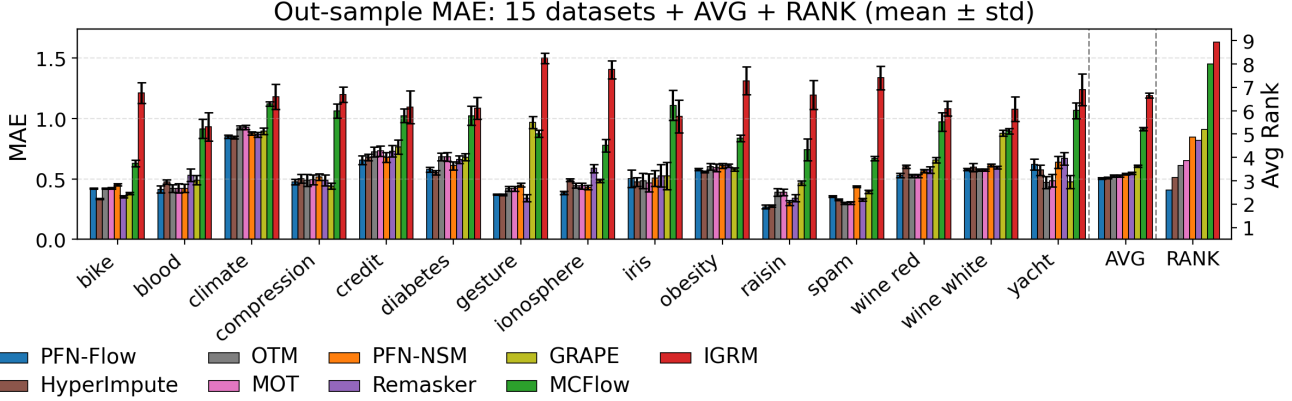


Figure 4. Imputation benchmark under MCAR missingness: out-of-sample MAE over 15 datasets, plus AVG and RANK (mean \pm std over masks).

D. Additional Experiments

We report additional imputation experiments under the MCAR missingness mechanism.

Figure 4 summarizes out-of-sample MAE across the same 15 imputation benchmark datasets, together with the overall average (AVG) and the average rank (RANK).

We additionally compare (i) our method against boosting baselines, (ii) TabPFN/PFN-family variants, and (iii) top split baselines, in that order.

D.1. Regression results under MCAR missingness

Across the 15 datasets in Figure 4, PFN-Flow is consistently competitive under MCAR missingness. In particular, PFN-Flow tends to achieve either the best or near-best MAE on a majority of datasets, and remains in the top tier in terms of AVG and RANK, indicating both strong average performance and stable behavior across datasets and masks. We also observe that some baselines can be highly dataset-dependent (large performance variance across datasets), whereas PFN-Flow exhibits comparatively uniform improvements.

D.2. Boosting baselines

Figure 5 compares PFN-Flow with three standard boosting baselines (XGBoost/CatBoost/LightGBM, trained on the same MCAR-imputed data). Each scatter contains two panels corresponding to missing rate $\leq 10\%$ and $> 10\%$; for each dataset, the x-axis is PFN-Flow AUC and the y-axis is the baseline AUC. Points below the diagonal therefore indicate that PFN-Flow outperforms the baseline on that dataset/group, while points above the diagonal indicate the opposite. Overall, most points lie on or below the diagonal, suggesting that PFN-Flow remains competitive against strong non-neural baselines under MCAR, with only a small

number of datasets where boosting can be slightly better.

D.3. TabPFN variants and PFN-family baselines

Figure 6 further compares PFN-Flow to TabPFN (Raw) and a PFN-family baseline (PFN-NSM). We observe that the points are highly concentrated near the diagonal in both missingness regimes, indicating that PFN-Flow is broadly comparable to TabPFN/PFN-family methods on the same datasets under MCAR. Notably, in the higher-missingness group ($> 10\%$), the scatter remains close to parity with only a few outliers, suggesting that PFN-Flow does not rely on a narrow set of favorable datasets and maintains stable performance as missingness increases.

D.4. Top split baselines

Figure 7 reports the strongest split baselines selected from our splitting-based design space (Top-1 to Top-4), each corresponding to a *pipeline* of a predictive model (here, CatBoost) and a specific imputation module. Within each subfigure, the two internal panels again correspond to missing rate $\leq 10\%$ and $> 10\%$. For each dataset, the x-axis is PFN-Flow AUC and the y-axis is the baseline pipeline AUC; points below the diagonal indicate that PFN-Flow improves upon that strong split baseline. Across all four top pipelines, the majority of points remain on or below the diagonal, showing that PFN-Flow is competitive even against the best-performing split configurations. At the same time, the few points above the diagonal highlight that no single method universally dominates every dataset, motivating the need for robust imputation that generalizes across heterogeneous tabular domains.

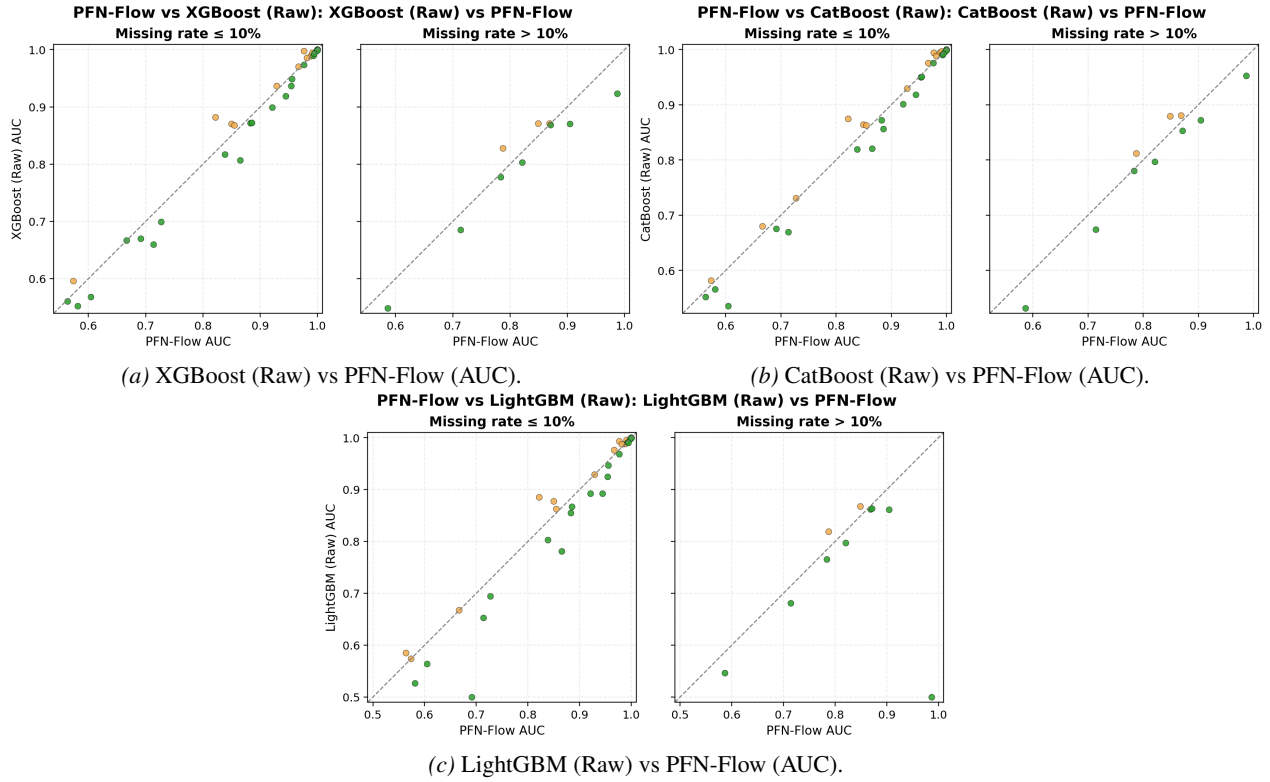


Figure 5. Boosting baseline comparisons against PFN-Flow under MCAR. Each point corresponds to one dataset in one missingness group; the diagonal indicates parity.

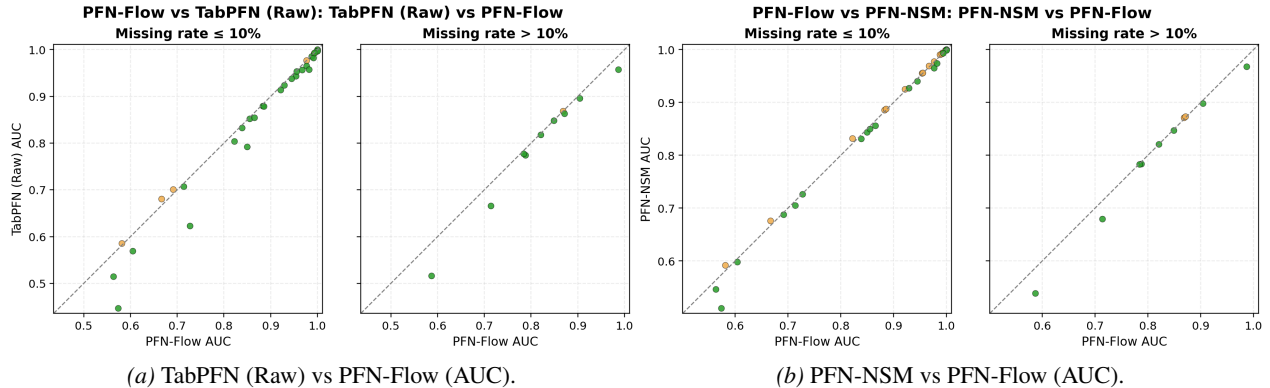


Figure 6. TabPFN/PFN-family comparisons against PFN-Flow under MCAR. Each point corresponds to one dataset in one missingness group; the diagonal indicates parity.

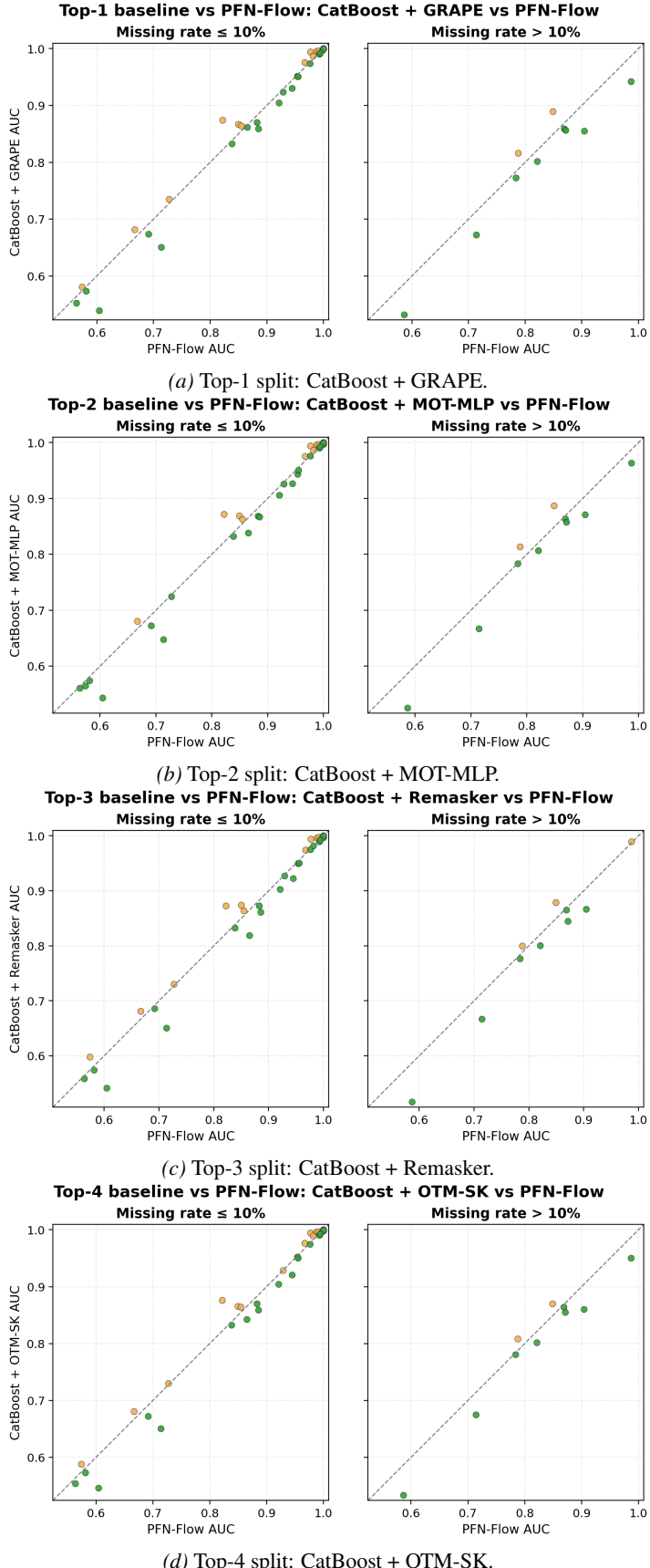


Figure 7. Top split comparisons.